

PAPER

Dynamics of dielectric barrier discharges in different arrangements

To cite this article: Valentin I Gibalov and Gerhard J Pietsch 2012 *Plasma Sources Sci. Technol.* **21** 024010

View the [article online](#) for updates and enhancements.

Related content

- [Development of dielectric barrier discharges](#)
Valentin I Gibalov and Gerhard J Pietsch
- [Dielectric barrier discharges in coplanar arrangements](#)
Valentin I Gibalov and Gerhard J Pietsch
- [Barrier discharges in coplanar electrode systems](#)
Valentin I Gibalov and Gerhard J Pietsch

Recent citations

- [Statistical behavior of a single microdischarge in atmospheric-pressure air dielectric barrier discharges](#)
Kun-Mo Lin *et al*
- [Lanthanum modified BFO-BT solid solutions: a structural, electrical and magnetic study](#)
C. Behera *et al*
- [Silicone-coated polyimide films deposited by surface dielectric barrier discharges](#)
Junggil KIM *et al*



IOP | ebooksTM

Bringing you innovative digital publishing with leading voices to create your essential collection of books in STEM research.

Start exploring the collection - download the first chapter of every title for free.

Dynamics of dielectric barrier discharges in different arrangements

Valentin I Gibalov¹ and Gerhard J Pietsch²

¹ Chemical Department, Moscow State University, Leninskij Gory, 11899 Moscow, Russia

² Institute for High Voltage Technology, RWTH Aachen University, Schinkelstr. 2, 52056 Aachen, Germany

E-mail: gibalov@medozone.ru and pietsch@ifht.rwth-aachen.de

Received 22 July 2011, in final form 28 February 2012

Published 4 April 2012

Online at stacks.iop.org/PSST/21/024010

Abstract

Based on experimental results, numerical investigations of dielectric barrier discharges (DBDs) have been performed in three basic configurations: in the volume, coplanar and surface discharge arrangements. It is shown that the DBD dynamics is the same in all arrangements and it is determined by the development of a few principal constituents, i.e. cathode- and anode-directed streamers, discharge channel, cathode layer and surface charges. It is found that the anode- and cathode-directed streamers appear with a highly conductive channel in between. The interaction of the streamers with conductive and dielectric surfaces determines the filamentary or homogeneous appearance of the discharge and its properties. The cathode-directed streamer is a self-sustaining phenomenon, which moves in a gas gap or along an electrode driven by a positive loop-back between photoemission and electron multiplication. The anode-directed streamer plays a subsidiary role. Depending on the kind of gas (electronegative or electropositive) and/or the degree of development of the cathode-directed streamer, the field strength in the conductive channels changes significantly. When the cathode-directed streamer touches the electrode surface, a cathode layer appears with parameters close to those of normal glow discharges. In volume discharge arrangements the movement of the streamers results in the appearance of Lichtenberg figures on dielectric surfaces.

(Some figures may appear in colour only in the online journal)

1. Introduction

Dielectric barrier discharges (DBDs) have been the focus of interest for more than a century. Two general features of DBDs, the non-thermal conditions in the discharge region and the technical simplicity of its realization, motivate the interest in this type of discharge. The range of applications covers, e.g., surface treatment, waste gas treatment, disinfection, deodorization, excimer lamps, CO₂ lasers and so on. This list has been extended recently to at least two more fields of interest: airflow control and medicine. However, water treatment (ozone generation) and plasma-display panels are still the most striking and extensive application areas of plasma-chemical technologies using DBDs. The latter has been intensively developed over the last two decades. The aim of this paper is not to give a full picture of all applications, but to provide a comprehensive understanding of the physical nature of DBDs in different arrangements.

DBDs are discharges where at least one of the electrodes is covered by a dielectric layer. With respect to fundamental features of DBDs numerous papers have been published recently concerning experimental as well as numerical results, e.g. [1–20]. Three basic configurations are known:

- (i) volume discharge (VD) arrangements where the discharge appears in a gas gap of flat parallel electrodes (figure 1(a));
- (ii) surface discharge (SD) arrangements with an elongated electrode on the surface of a dielectric and an extended counter-electrode on the reverse side of the dielectric; the discharge appears on the dielectric surface (figure 1(b));
- (iii) coplanar discharge (CD) arrangements with one or several pairs of parallel electrodes embedded in a dielectric near a surface with the discharge on the surface of the dielectric (figure 1(c)).

Additionally, two cases can be distinguished: a symmetrical one with both electrodes covered by a dielectric

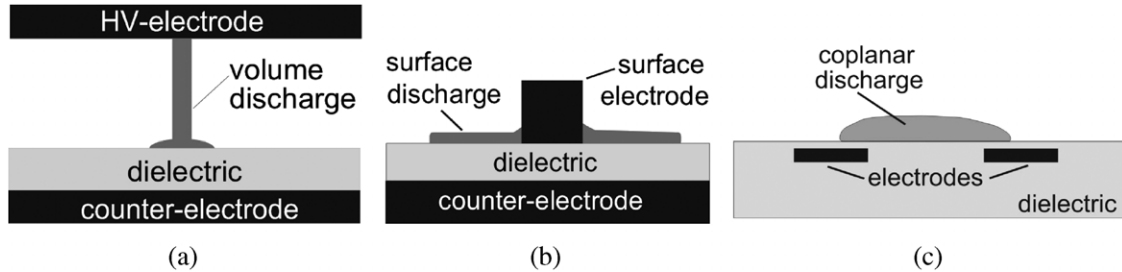


Figure 1. Basic configurations of DBDs: (a) VD, (b) SD and (c) CD arrangements.

('dielectric electrodes' in arrangements (i) and (iii)) and an asymmetrical one with a conductive and a dielectric electrode (arrangements (i) and (ii)). The asymmetry of the electrodes affects the discharge development, its final parameters, and consequently the efficiency of certain applications (e.g. [21–23]). The discharge structure changes significantly, depending on the arrangement of the electrodes.

Non-thermal conditions in DBDs mean that electrons are not in equilibrium with heavy particles. The electron energy is a few orders of magnitude higher than that of the neutrals and ions. Because of this, the DBD becomes an effective source of radicals and excited particles.

The most common DBD configuration is the VD arrangement. The discharge occurs in a gas gap, which has a width of most often a few millimetres. In general, the discharge consists of a set of transient tiny discharge columns (microdischarges) and surface discharges on the dielectric(s). Under certain conditions the tiny columns increase their cross-section, merge, and the discharge appears to be homogeneous.

In the second basic configuration, the surface barrier discharge (SD) arrangement, the discharge develops along the dielectric surface. At critical field strength a set of microdischarges appears on the dielectric surface. The SD develops in an initially decreasing field strength distribution, while the numerous microdischarges in VD arrangements develop in uniform background field strength. The duration of the microdischarge development is comparable to that in VD arrangements.

The last basic configuration is the CD arrangement. The electrodes (strips) can be produced with high accuracy and easily be coated with a dielectric layer by technologies well known in the semiconductor industry. Short inter-electrode gaps in the range of $100\ \mu\text{m}$ and less can be realized. At short inter-electrode gaps the discharge behaves similar to VDs. Microdischarge channels bridge the region on the dielectric surface above the electrodes. The discharge patterns are independent of polarity. The length of the channels is basically fixed and is in the range of the inter-electrode gap. The CD, especially with short electrode gaps, combines in some way the properties of VDs and SDs. It develops in a more uniform initial field strength than the SD.

The terms 'streamer' and 'microdischarge channel' or 'channel' are used in this paper. The meaning of these terms is as follows: the streamer is a compact, moveable structure, which is linked to a field strength distortion. The

microdischarge channel is the highly conductive region that is left behind the streamer and is a result of the streamer development and propagation.

The aim of this paper is to review the mechanisms governing the dynamics and breakdown of DBDs in VD (section 2), CD (section 3) and SD arrangements (section 4). In section 5 some generalizations of the discharge development in these arrangements and features of the cathode- and anode-directed streamers, of Lichtenberg figures, cathode layers, filamentary and homogeneous discharge structures and of microdischarge channels are provided. The numerical results are based on experimental findings as far as available. If not otherwise mentioned, all investigations are performed for DBDs in air or oxygen at atmospheric pressure and a gap distance of typically 1 mm. The arrangements are fed by an ac voltage with a frequency of up to a few kHz or pulse voltages with comparable rate of voltage rise, i.e. the rate of voltage change is significantly lower than 1 kV ns^{-1} . Under this condition physical processes in DBDs are faster than the voltage change; breakdown follows according to Paschen's law and the shape of the applied voltage and its amplitude do not affect the breakdown process.

2. Volume barrier discharge

2.1. Experimental findings

In general, the volume barrier discharge consists of numerous microdischarges. Their channels cross the gas gap and connect the cathode with the anode (figure 2, [21–23]). Typical values of the duration of a microdischarge and the size of its channel are provided in the figure. The structure of the channel and its temporal development depend on the type of electrode (dielectric or conductive) and its polarity.

It is obvious that a cathode-directed streamer is a precursor of channel formation. Emission appears somewhere in the middle of the gas gap, closer to the anode, and spreads to the cathode. A dark region appears behind the head of the cathode-directed streamer in any arrangement. This means there are either no electrons or the field strength is close to zero in this region.

An anode-directed streamer exists as well. It appears a few nanoseconds after the cathode-directed one. If the anode is non-conductive the discharge spreads over the anode surface (figures 2(a) and (c)). A similar spreading appears on the dielectric cathode (figures 2(a) and (b)).

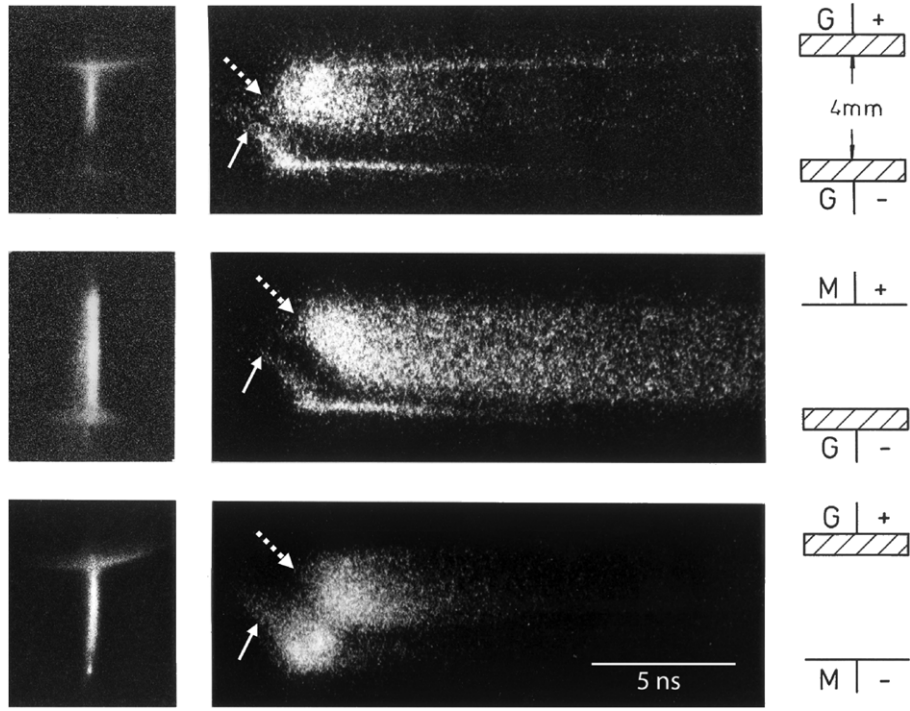


Figure 2. Still (left) and streak photographs (right) of a single microdischarge channel in air at atmospheric pressure (the gas gap is 4 mm; G is glass and M is metal, and polarity is given on the right-hand side; the full line arrows mark the cathode-directed and the dotted arrows the anode-directed streamers [21–23].

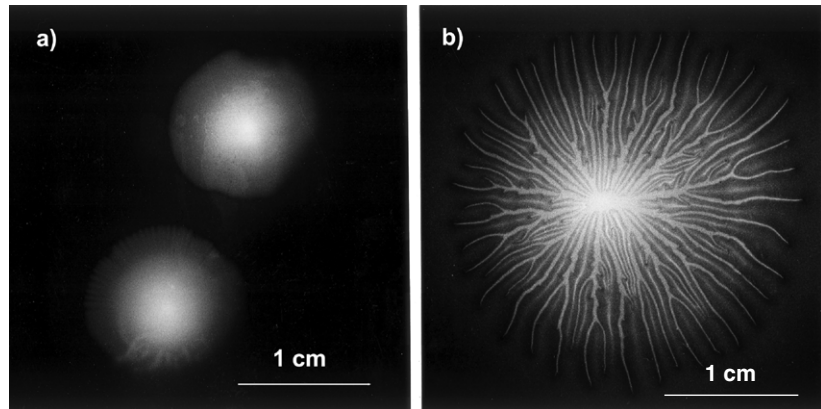


Figure 3. Discharge patterns of VDs on the dielectric surface: (a) discharge structures on the anode (from two microdischarges); (b) Lichtenberg figure on the cathode (dry air of 1 bar, gap distance 2 mm, metal–glass configuration, voltage pulse with a peak value near breakdown voltage in the gap).

Initially, the light emission is connected with the propagation of the streamers. Later, when the streamers touch the electrodes, the channel starts to radiate. The duration of light emission is shorter in cases with a dielectric anode (figures 2(a) and (c)). It seems that charge (i.e. electron) accumulation on the dielectric anode extinguishes the discharge activity in the gas gap.

The pattern of the channel footprint on the dielectric electrode depends on polarity. In the case of a dielectric cathode, distinct channels spread out from the discharge axis on the dielectric surface. At the dielectric anode a homogeneous, diffuse discharge area is observed with a distinct boundary on the dielectric (figure 3).

If the anode is conductive the duration of light emission is several times longer than that with a non-conductive one

(figure 2(b)). Moreover, the radiation takes place in the whole discharge gap from the cathode to the anode. Additionally, the cross-section of the channel is wider compared with the other cases (figure 2(b)). The spreading of the discharge near the dielectric cathode (bright, narrow zone near the cathode) is due to the development of a surface discharge over the dielectric surface (figures 2(a) and (b)).

2.2. Value of transferred charge

It has been found that in electronegative gases a certain amount of charge is transferred through each microdischarge channel, e.g. [24]. Sets of microdischarges appear practically simultaneously in the discharge gap and cause a voltage jump in the external circuit. The frequency of appearance (probability)

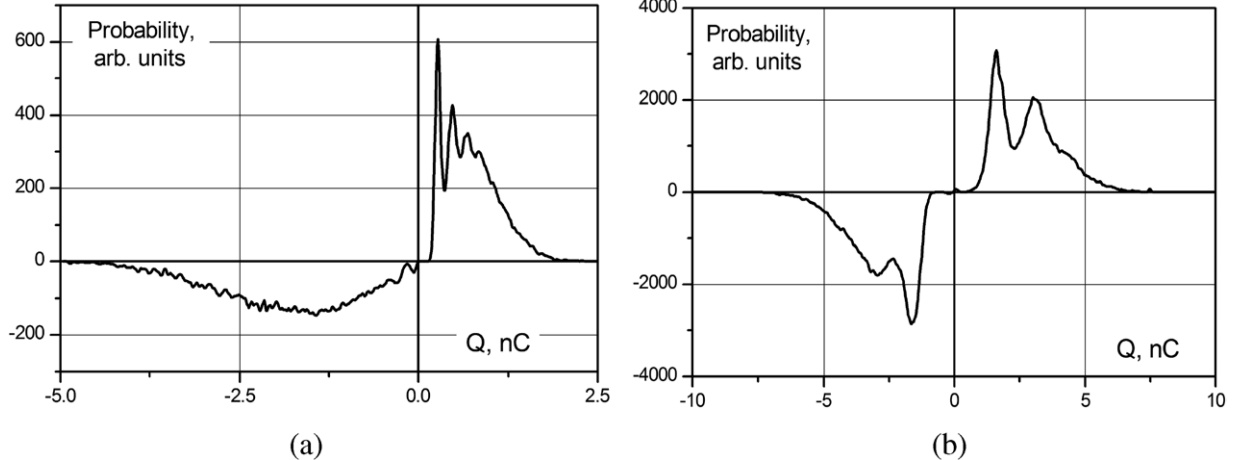


Figure 4. Probability of the appearance of sets of microdischarges against the value of the transferred charge in an asymmetric VD arrangement in oxygen of normal pressure, (a) discharge gap 1.4 mm, dielectric glass ($\epsilon_r = 5$), (b) discharge gap 0.18 mm, dielectric ceramic ($\epsilon_r = 150$) (positive charge values mean the dielectric is the anode).

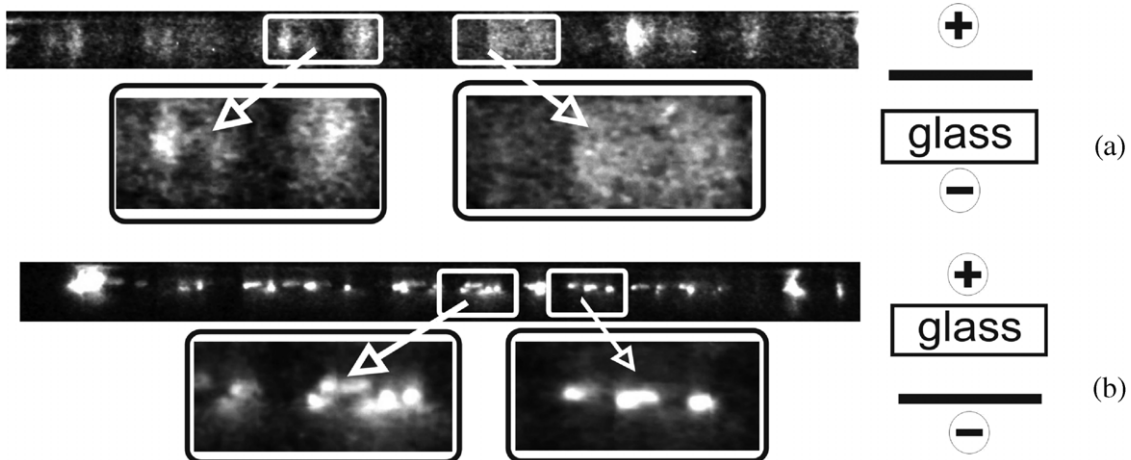


Figure 5. Photographs of a volume discharge in an asymmetric arrangement (discharge gap 0.7 mm, air of 1 bar, exposure time 20 ms); polarity of the dielectric (a) negative and (b) positive; the arrows show enlarged sectional views.

of such jumps over the transferred charge is given in figure 4 for an asymmetric VD arrangement in oxygen at atmospheric pressure with an electrode diameter of 20 mm. Usually, the probability distribution has several maxima (figure 4(a), positive charges). An additional microdischarge in a set causes an additional maximum in the curve. The charge value, which is transferred through a single microdischarge channel, is just the difference between two adjacent maxima. For example, this value is 0.18 nC for a discharge gap of 1.4 mm and a relative permittivity $\epsilon_r = 5$ (glass), and 1.4 nC for a discharge gap of 0.18 mm and $\epsilon_r = 150$ (ceramic).

In the case where the dielectric is the cathode (figure 4(a), negative charges), channels with distinct values of transferred charge do not appear. The transferred charge has a wide distribution with only a single broad maximum. The same behaviour is observed in the pictures of a discharge in an asymmetrical arrangement (figure 5). The discharge region is filled by a broader, more homogeneous and faint discharge structure (figure 5(a)). In the case where the dielectric is the anode, a filamentary structure exists (figure 5(b)). This result seems to be not in agreement with what is observed

in figure 2, where a filamentary structure is observed at both polarities.

The experiments for figure 2 were performed in an arrangement with rod electrodes with spherical tips and a comparatively large electrode gap. In this case the discharge is forced to be concentrated on the axis of the arrangement. Nevertheless, a certain enlargement of the discharge cross-section is observed in the case of dielectric cathode in figure 2(b) as well. Obviously, this phenomenon results from the asymmetrical electrode configuration, i.e. only one electrode is covered by a dielectric.

The asymmetry of the probability distribution in figure 4(a) disappears if the relative permittivity of the dielectric changes from 5 to 150 (figure 4(b)). The value of the transferred charge is several times larger in the latter case. It is necessary to stress that a transition from (more or less) homogeneous charge transfer to a filamentary one takes place under the same experimental boundary conditions, e.g. the diameter of the electrode, applied voltage, type of feed gas and so on are identical, except the relative permittivity. From a physical point of view a tremendous increase in the permittivity

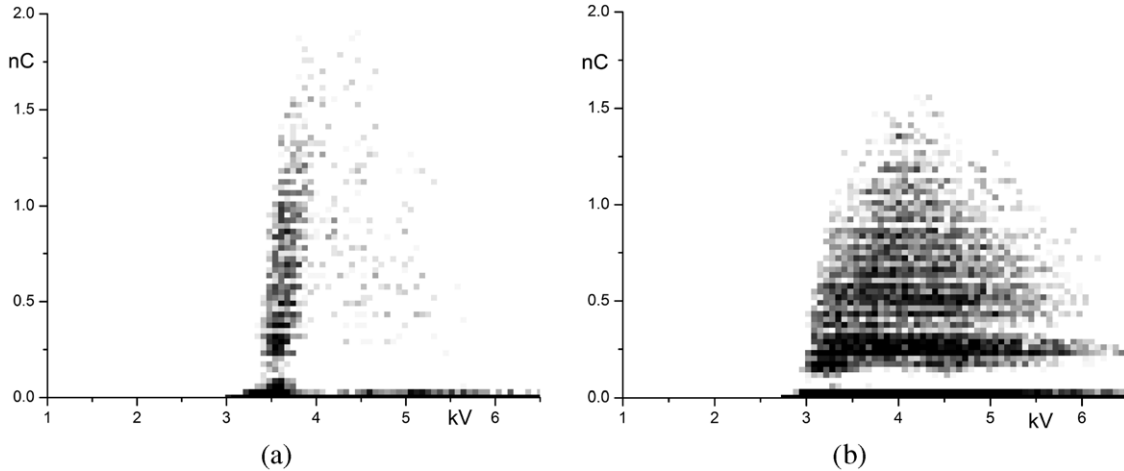


Figure 6. Transferred charge over applied voltage for negative (a) and positive (b) polarity of the dielectric electrode (dielectric–metal arrangement, discharge gap 1.2 mm, thickness of the dielectric 4 mm, relative permittivity 5, air of atmospheric pressure, amplitude of the applied voltage 6.5 kV [25].

means the electrical properties of the dielectric approach those of a conductor. Asymptotically, a conductor is a dielectric with infinite permittivity, which means there are no surface discharges on the electrode, and the discharge structure in the gas gap becomes a filamentary one.

2.3. Dynamics of charge transfer

As shown above, in asymmetric VD arrangements the charge transfer happens either in homogeneous or filamentary discharge structures. There exists a certain asymmetry in the temporal distribution of the charge transfer process as well (figure 6). With rising voltage microdischarges occur, when breakdown voltage is reached, combined with a charge transfer. After the extinction of the microdischarges, the mean field strength in the discharge gap decreases due to the charge accumulation on the dielectric surface. With further rising voltage, breakdown conditions are reached again in the discharge gap. So, charge transfer takes place continuously up to the voltage maximum in accordance with figure 6(b).

Experiments with asymmetric discharge arrangements, however, highlight the temporal asymmetry of the charge transfer process (figure 6). For both polarities discharges appear at the same voltage during continuous operation. If the dielectric electrode is the cathode, the discharge transfer happens in a narrow time interval near the breakdown voltage (~ 3.5 kV in figure 6(a)). After this, further voltage rise up to the voltage maximum (6.5 kV) hardly contributes to a further charge transfer. In this half-period of the applied voltage the charge transfer happens at about 3.5 kV in a homogeneous structure (figure 5(a)). This means that the average field strength in the discharge gap drops to zero and does not reach breakdown conditions again up to the maximum of the applied voltage (6.5 kV) in the given arrangement.

If the dielectric electrode is the anode, current pulses occur continuously in the gas gap from the breakdown voltage up to the voltage maximum (figure 6(b)). This mechanism of charge transfer is connected with the filamentary discharge

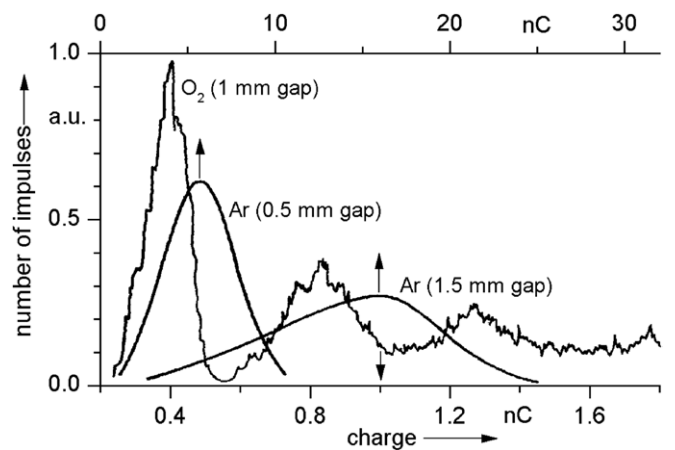


Figure 7. Frequency distribution of transferred charges in a VD arrangement in oxygen and argon [25].

structure (figure 5(b)). Microdischarges appear locally where breakdown conditions are reached. With rising voltage, breakdown conditions are reached first at locations in between accumulations of surface charges from preceding sets of microdischarges on the dielectric. Only a comparatively small voltage rise is needed for further discharge activity, i.e. microdischarges occur continuously up to the voltage maximum. Depending on the voltage amplitude they cover the dielectric surface and may even discharge areas, which have already been discharged once in a half-period of the applied voltage.

The mechanism of charge transfer in DBDs in a filamentary and homogeneous mode is determined by the discharge configuration, first of all the kind of electrode material, polarity and electrode distance. The type of gas also influences the charge transfer (discharge structure). In electropositive gases like argon no distinct filaments appear (figure 7). The charge transfer in, e.g., nitrogen or argon is characterized by a broad charge distribution with a single maximum in contrast to the multi-extrema curve in oxygen (figure 7).

2.4. Modelling of VDs

In order to understand the dynamics of the discharge a self-consistent, two-dimensional modelling was performed for a volume barrier discharge with a conductive cathode and a dielectric anode (gas gap 1 mm, oxygen of 1 bar [26]).

Modelling of the discharge means calculation of the temporal behaviour of the electric field distribution in the discharge gap simultaneously with the dynamics of the charged particles. The numerical model is based on the assumption of local equilibrium, e.g. drift parameters of the charged particles and the reaction rate constants depend on the local field strength. The microdischarge channel is assumed to be radially symmetric.

2.4.1. Transport equations, initial and boundary conditions. In general, the dynamics of charged and neutral particle densities is described by a system of Boltzmann equations. A direct solution is time consuming, while the results do not differ significantly from those of the indirect solution [27, 31]. That is why the local field approximation (LFA) [19, 20, 27, 28, 30, 32–34] is used here. The system of continuity equations, describing the spatial and temporal distribution of all particles, consists of

$$\begin{aligned} \frac{\partial n_i}{\partial t} + \operatorname{div} \vec{j}_i &= S_i \\ \vec{j}_i &= -D_i \cdot \operatorname{grad} n_i + \vec{v}_i \cdot n_i \end{aligned} \quad (1)$$

where n_i , j_i , S_i , D_i and v_i are the number density of charged particles, current density, source term, diffusion coefficient and drift velocity of the i th component of the plasma. The discharge development is modelled in oxygen. The following neutral and charged particles are included: O_2 , O_3 , O , O_2^+ , O_2^- , O^- and electrons. The list of reactions between these particles includes ionization, attachment and detachment processes, dissociation of O_2 and O_3 by electron impact, photoionization and photoemission from the surfaces [35]. The modelling is performed for an arrangement with a gas gap of 1 mm, a thickness of the dielectric layer of 2 mm on the anode and a relative dielectric permittivity of 5 [26, 35].

In order to solve this system the initial and boundary conditions must be fixed. There are two types of boundaries: at the surface of the electrodes, and those which limit the integration region in the gas space (external boundaries). The solid surfaces are considered as areas which adsorb particles and as a source of secondary electrons. They are released by photon and ion impact processes. The resulting flux of secondary electrons is given by

$$n_e \cdot v_e = \gamma_+ \cdot n_+ \cdot v_+ + \gamma_{ph} \cdot \phi. \quad (2)$$

The photon flux density ϕ on the surface is taken to be proportional to the ionization rate and can be determined by integration over the whole discharge volume [36, 37]. The emission coefficients (γ_+ and γ_{ph}) are varied during modelling from 0.001 to 1.0. Adapting theoretical to experimental current

developments in shape and amplitude, γ_{ph} values in the range 0.1–0.3 are found.

The following initial conditions are set:

- the initial electron-ion pairs (seed electrons) are homogeneously distributed in a layer near the cathode with a maximum density in the range 10^7 – 10^8 cm $^{-3}$;
- the net charge in the gas region is zero,
- the initial charge density on the dielectric surface is zero.

The drift velocities of the charged particles and the ionization as well as the attachment-detachment coefficients are taken as functions of the reduced field strength E/n from [38]. The continuity equations are solved by an explicit method. To compensate or limit the numerical diffusion a flux-correction-technique algorithm [39–41] is applied.

2.4.2. Field calculation. The field distribution is obtained as a solution of the Poisson equation:

$$\operatorname{div} \vec{E} = \frac{\rho_i}{\epsilon_0 \cdot \epsilon_i} \quad (3)$$

where ϵ_i is the relative permittivity and ρ_i the total charge density of the corresponding region. The Poisson equation is solved by a cyclic reduction algorithm of the linear system of equations that results from a 2D finite difference approximation [42] with the following boundary conditions:

- the potential on the conductive anode and cathode is known (breakdown voltage);
- the potential on the dielectric surface of the anode is determined taking into account the surface charge density, which is accumulated during the discharge development;
- the field strength far from the channel axis is homogeneous;
- the derivation of the field strength on the channel axis is zero, i.e. the microdischarge is assumed to be axis-symmetric.

2.4.3. Initial phase of discharge development. The charge transfer in the discharge gap of a VD arrangement starts with initial (seed) electrons in a homogeneous field. The first avalanche slightly distorts the electric field during its movement (figure 8, 2 ns); however, the homogeneous background field still determines the discharge development. The slight distortion is more pronounced when more avalanches approach the anode (figure 8, 4 ns). The field enhancement on the cathode side of this distortion is of importance for further development of the discharge (figure 8, 6 ns).

Secondary electrons from detachment and photoemission processes, which appear in the region between the cathode surface and the field distortion, move through the field strength distortion, where they multiply their number and increase the intensity of the photoemission process. As a result, the field strength between the distortion and the anode (figure 8, 6 and 8 ns) decreases, the field distortion is shifted towards the cathode and a cathode-directed streamer appears.

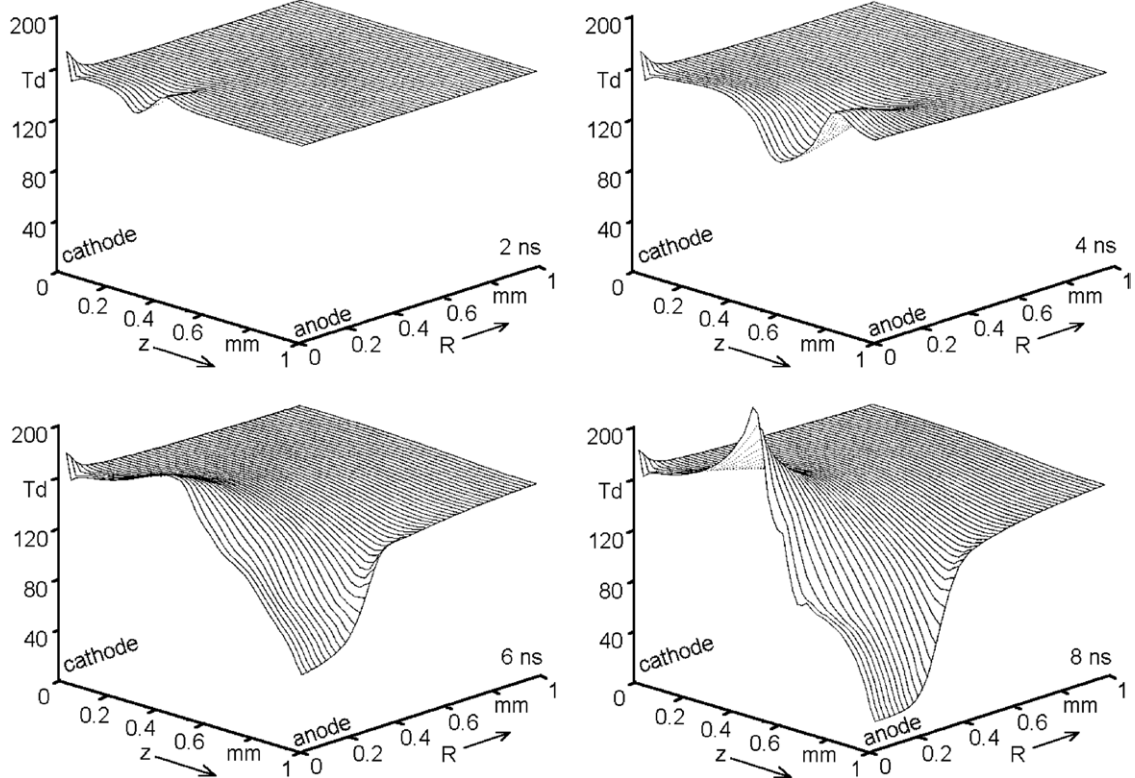


Figure 8. Temporal development of the axial electric field strength component in a VD arrangement during the initial phase of the discharge (applied voltage 4.5 kV).

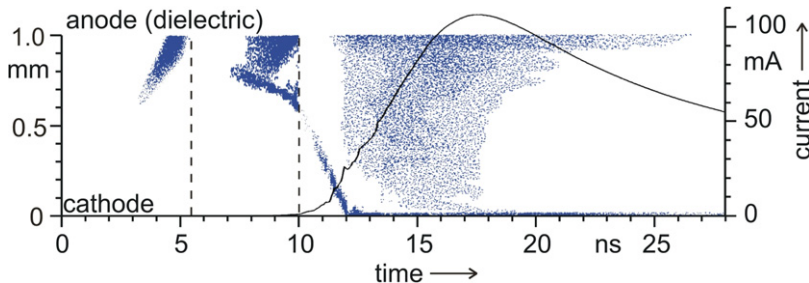


Figure 9. Simulated streak photo of a microdischarge (light emission proportional to the density of dots) and synchronized discharge current (solid line); the sensitivity is reduced at 5.5 and 10 ns.

2.4.4. Streamer phase. In VD arrangements the number density of secondary electrons, which appears due to photoemission processes, is high enough to initiate a self-sustaining process. The enhanced field distortion and thus the rising ionization rate create more and more charge carriers. The increased production of charge carriers causes a further field enhancement in the distortion and accelerates its propagation towards the cathode. This phenomenon has been observed experimentally and is known as the cathode-directed streamer. This propagation can be seen in the simulated streak picture of the temporal development of light emission (figure 9), which is comparable to the experimental results in figure 2.

The velocity of the cathode-directed streamer and the axial field strength component reach the highest values near the cathode surface. After reaching the surface a cathode layer develops with a normal current density of about 200 A cm^{-2} . The cross-section of the cathode layer increases and supports

the rise in the discharge current (compare figure 9 with 10). The velocity of the radial expansion of the cathode layer cross-section determines the steepness of the current rise.

2.4.5. Charge transfer phase and discharge decay. Simultaneously with the cathode layer expansion the main portion of the charge is released in the gas gap. The amplitude of current determines the amount of the transferred charge. This amount depends on the boundary conditions, first and foremost, the dielectric constant (figure 11).

With rising current the field strength in the channel decreases. It decreases down to a value of about 100 Td (in oxygen), which is close to the level where the effective ionization coefficient is zero. At this level the ionization rate is equal to the attachment rate. The size of the region with reduced field strength, which determines the discharge current (figure 11), depends on the dielectric constant (figure 12).

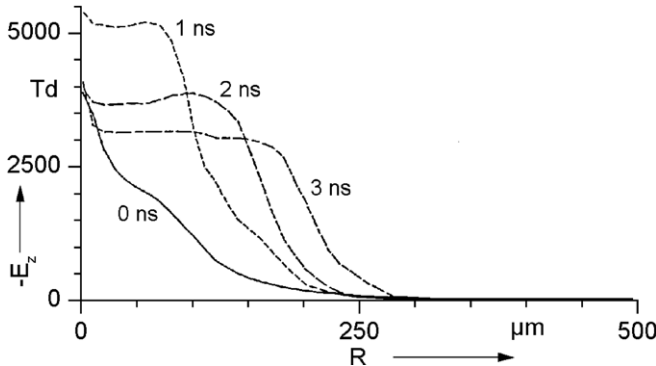


Figure 10. Radial expansion of the cathode layer (VD arrangement; $t = 0$ corresponds to $t \approx 12$ ns in figure 9 [26]).

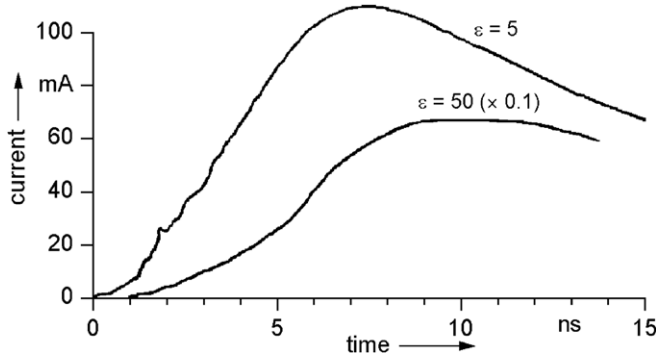


Figure 11. Discharge current for two values of the dielectric constant (VD arrangement, oxygen of 1 bar, gas gap 1 mm, thickness of the dielectric layer on both electrodes 2 mm, relative permittivities of the dielectric 5 and 50, respectively).

The radius of the microdischarge channel is approximately proportional to the square root of the value of the relative dielectric permittivity (0.3 mm for $\epsilon_r = 5$ and 0.8 mm for $\epsilon_r = 50$).

The cathode layer expansion stops before the current reaches its maximum (compare figure 9 with 11). When the cathode layer reaches its maximum size, the diameter of the discharge channel does not grow any further. Its shape can be clearly seen in figure 12; it is a real channel, which transfers charges from the cathode layer to the surface of the anode. The main transfer happens 6–8 ns after the cathode-directed streamer touches the cathode surface. Within this time interval the channel radiates (figure 9).

The charge transfer supports the propagation of the anode-directed streamer (figure 13). The streamer reaches the anode before the cathode-directed one touches the cathode at about 10 ns (figures 9 and 13). Due to permanent feed of the anode-directed streamer by charges from the channel, it propagates radially along the anode surface. This is obvious from modelling results (figure 13) as well as experimental findings (figures 2(a) and (c)). Finally, the anode-directed streamer leaves charges on the anode surface with a radius of about 1 mm or more; that is four times larger than the radius of the cathode layer and microdischarge channel (figures 10, 12 and 13(a)). The charge density at the anode is nearly constant (about 20 nC cm^{-2}). The potential of the charged anode decreases to nearly 50% of the initial level (figure 13(b)).

The growing charge density on the dielectric anode causes a decrease in the average field strength in the discharge gap down to extinction value (screening effect). Breakdown conditions can be reached again by an increase in the applied voltage. This sequence of (i) breakdown in the gas gap, (ii) decrease in field strength and (iii) reaching breakdown conditions again by voltage rise starts at the ignition voltage and runs up to the voltage maximum in each half-period.

Charge accumulation on the dielectric anode combined with the decrease in the local field strength has a further effect; it screens the space around the discharge channels and by this suppresses the development of adjacent ones. That is why succeeding microdischarges appear with rising voltage in between the charged areas of the preceding ones. The larger the distance between adjacent microdischarges the weaker is the interaction between the channels and more charge can be transferred through the microdischarge channel. If the distance between channels is large enough (compared with the channel diameter) the value of the transferred charge reaches its maximum (figure 14, $X/D \approx 15\text{--}30$, equivalent to an inter-channel distance of about 4–10 mm). The closer the channels, the smaller is the charge through a channel, which reaches the anode; however, the average charge density (at the anode) from all channels rises up to a saturation level. The probable distance between adjacent microdischarges at the beginning of the saturation density of the surface charge is $X \approx 0.9\text{--}1.0$ mm (at $X^2/D^2 \approx 5\text{--}6$ in figures 14 and 10).

2.5. Discharge energy

In general, at atmospheric pressure the energy is released in microdischarge channels within a time period of about 50 ns. Energy consumption starts with the appearance of initial electrons and lasts over all phases of charge transfer up to the decay of the microdischarge. However, the amount of energy released and the portion, which can be used, e.g., for the generation of radicals, are quite different during the discharge phases.

The main part of energy is released in the microdischarge channel during the current pulse (figure 11). The distribution of the total amount of energy accumulated in the gas gap up to 32 ns is given in figure 15.

There are two maxima in the energy density distribution, in the cathode layer and in the middle of the conductive channel (figure 15). The first one belongs to energy dissipation of positive ions in the cathode layer. The second maximum can be explained as follows: electrons originating from the cathode layer are accelerated in the discharge channel causing a growth of the electron and energy densities. Approaching the anode the channel diameter grows (figure 13), reducing the electron and energy densities, so that in between the cathode and anode a maximum of the energy density must appear.

The specific heat capacity of oxygen under normal conditions is roughly 1 mJ cm^{-3} . Hence, the maximum temperature jump at the centre of the cathode layer is nearly 350°C (figure 15). This value is reached in a rather limited area. In the channel, the temperature jump does not exceed

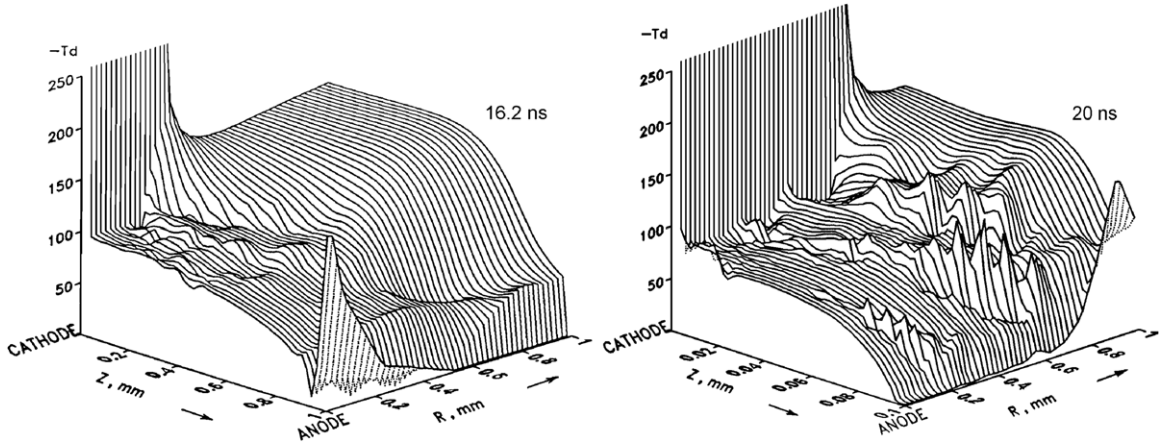


Figure 12. Total field strength configuration of microdischarge channels with a relative dielectric constant of 5 (a) and 50 (b), respectively (the channel axis is in the z -direction).

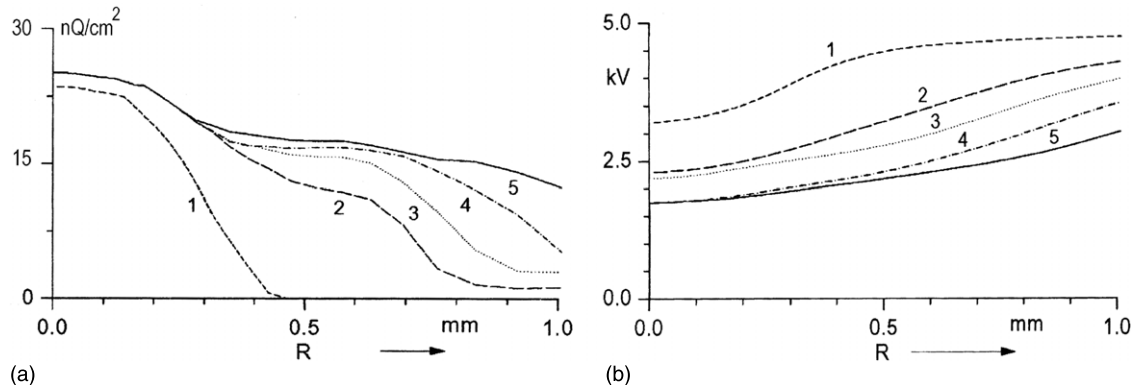


Figure 13. Distributions of (a) the surface charge density and (b) the surface potential on the dielectric anode (VD arrangement); time: 1—10.7 ns; 2—13.9 ns; 3—15.5 ns; 4—17.9 ns; 5—32.3 ns.

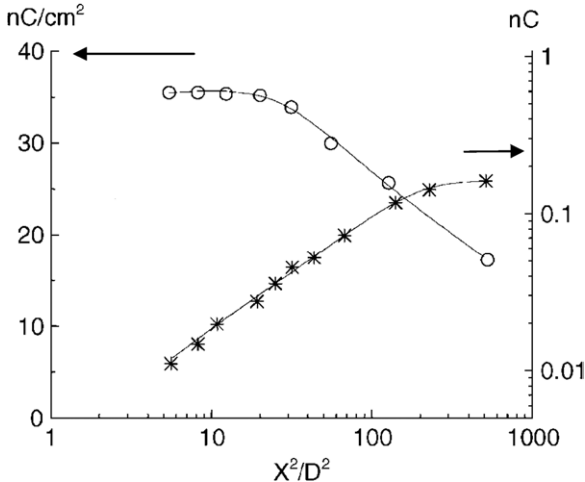


Figure 14. Mean surface charge density (circles, left axis) and transferred charge (crosses, right axis) over the square of the relative inter-channel distance (X : inter-channel distance, D : channel diameter; for a gas gap of 1 mm and oxygen at atmospheric pressure).

a value of about 10°C on average (figure 16). About 40% of the energy is released in the cathode layer. This amount of energy can be easily removed to the cooling system of the discharge unit.

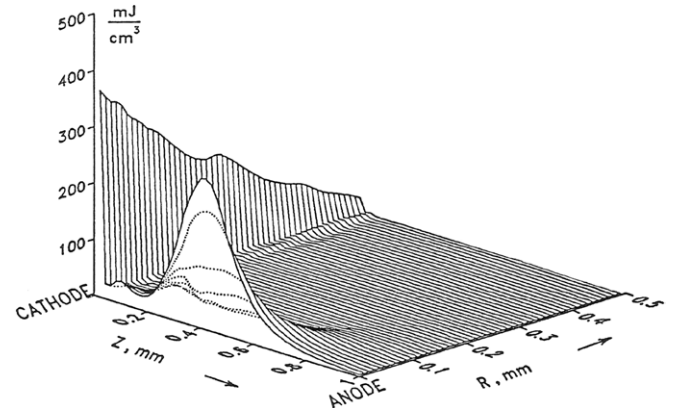


Figure 15. Energy density distribution in the gas gap of a VD arrangement in the decay phase of the current (at 28 ns in figure 9; oxygen of atmospheric pressure, gas gap 1 mm).

3. Coplanar barrier discharge

3.1. Experimental findings

In general DBDs develop in a gas volume and/or on dielectric surfaces. The DBD in volume arrangements is characterized by a defined discharge length, i.e. gas gap and a uniform initial field strength distribution. The DBD on surfaces extends over a

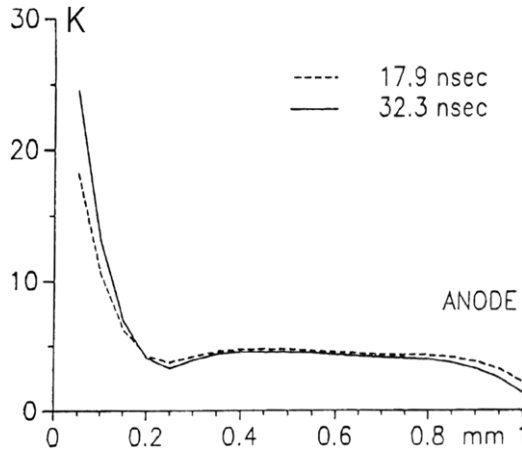


Figure 16. Average temperature jump in a microdischarge channel of a VD arrangement in oxygen of atmospheric pressure and a gas gap of 1 mm.

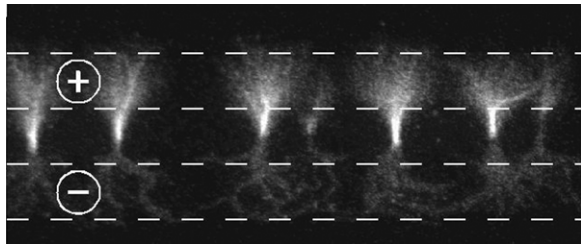


Figure 17. Top view on a coplanar discharge in air under ambient conditions; the location of the electrodes is marked by dashed lines, the inter-electrode distance is 2 mm and the exposure time corresponds to a half-cycle of the applied voltage [47].

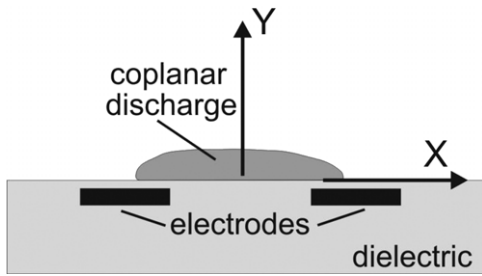


Figure 18. Sketch of a CD arrangement.

distance, which is not defined by the geometrical configuration (but rather by the amplitude of the applied voltage) and is characterized by an extremely non-uniform initial field strength distribution. The DBD in coplanar arrangements takes a position in between; it has a more or less well-defined inter-electrode distance (on the surface) and the initial field strength is non-uniform.

Coplanar (barrier) discharges (CDs) appear in general in arrangements where a dielectric layer covers a pair (or several pairs) of long, parallel electrodes placed on a dielectric plate (figure 1(c)). The discharge develops on/above the dielectric layer in the form of discharge channels, which cross the area above the electrodes (figures 17 and 18). Usually, the electrode gap is of the order of $100\text{ }\mu\text{m}$ and the thickness of the dielectric layer is typically about $10\text{--}60\text{ }\mu\text{m}$ depending on the application.

Table 1. Parameters of the CD arrangement under investigation.

| Parameter | Values |
|--|---------------------------|
| Electrode distance | $80\text{ }\mu\text{m}$ |
| Thickness of the dielectric layer ^a | $55\text{ }\mu\text{m}$ |
| Width of the electrodes | $120\text{ }\mu\text{m}$ |
| Relative permittivity of the dielectric | 10 |
| Thickness of the dielectric block | $1000\text{ }\mu\text{m}$ |
| Thickness of the electrodes | $5\text{ }\mu\text{m}$ |

^a Above the electrodes.

The distinct parallel discharge channels originate and terminate at the locations of the electrodes on the dielectric surface (figure 17). The average distance between the channels is on the order of the inter-electrode distance. The channels seem to appear simultaneously in series of microdischarges and develop rather independently from each other. Channels from preceding series influence the succeeding ones by surface charges left on the dielectric surface.

There are plenty of papers dealing with the experimental investigation of CDs and their numerical modelling. The majority of them address plasma display panels (PDPs) [28–30]. However, only a small number of experimental [43–48] and modelling [49–51] results refer to CDs in electronegative gases.

3.2. Numerical model

The numerical model of the CD is based on experimental findings with parameters presented in table 1. If not otherwise mentioned, the default values are taken for modelling in an oxygen environment of 1.7 bar and with an applied voltage of 2100 V.

The physical model of the CD and the mathematical formalism of the modelling are close to the model of the VD, which is adapted to the surface geometry. The charge dynamics is described by a set of continuity equations, which are solved two-dimensionally. The xy -plane crosses a channel along its length (figure 18).

The width of the channels is small in comparison with the inter-channel distance (figure 17). The two-dimensional (2D) approach allows one to obtain reliable results with comparably low methodical difficulties. The discharge is taken as being uniform in one dimension (along the length of the electrodes, the z -coordinate). The transport equations (in orthogonal coordinates, without radial symmetry) and the initial and boundary conditions are similar to those for the VD case. The discharge current and energy are calculated using experimental values of the width of the discharge channels (in the z -direction). The chemical code is the same as that used to model VDs.

3.3. Field calculation

The field calculation for CD arrangements differs significantly from that for VDs. The CD develops in the immediate vicinity of the dielectric surface. That is why the boundary conditions, which are necessary to solve the Poisson equation, must be determined with high accuracy. The CD arrangement consists

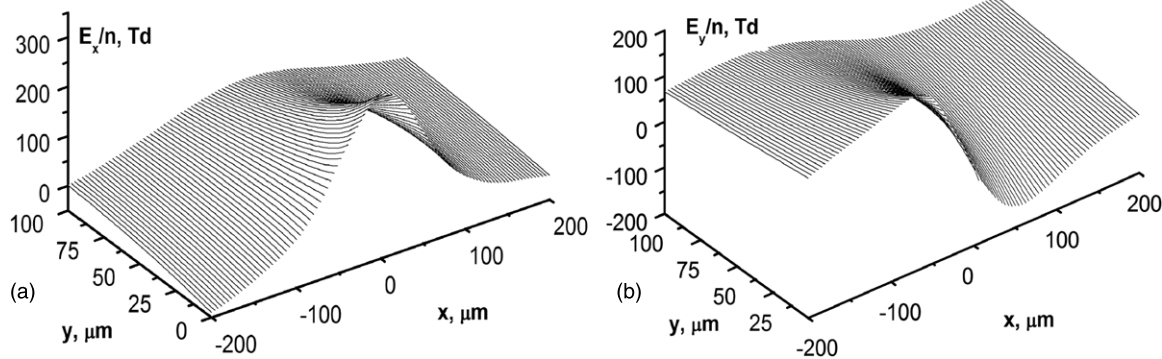


Figure 19. Initial field strength distribution above the dielectric surface, (a) tangential and (b) normal component of the field strength ($x = 0$ is the location in between the electrodes on the dielectric surface; for boundary conditions and dimensions see section 3.2).

of two regions with different permittivities (gas region and dielectric plate). The Poisson equation (3) must be solved in both of them to find the field configuration.

The field strength distribution in the discharge region is calculated by the differential grid method with a homogeneous grid and known potential on the boundaries, which surround the discharge region [42]. The main methodical effort is directed to the precise definition of the boundary conditions, which are calculated three-dimensionally. To do this, three groups of real charges are considered: in the discharge volume (gas space), on the dielectric surface and on the surface of the conductive electrodes.

There exists a precise solution of the Poisson equation for a point charge within stacked dielectric layers. The solution can be presented as a sum of the initial charge and an infinite number of image charges. The positions and values of the image charges are determined by the thickness of the dielectric layers and their permittivity (e.g. [52]).

In summary, three groups of charges, which consist of real charges and a certain number of image charges, form the overall charge ensemble. The pair of conductive electrodes and the dielectric block are substituted by an ensemble of charges. The potential at each point of the boundary of the integration region is the sum of the partial potentials of each charge from the charge ensemble.

In order to determine the potential, the value of each charge of the ensemble must be known. Two groups of real charges in the model (the charges in the discharge region and on the dielectric surface) are obtained as a solution of the set of continuity equations at each time step. The image charges necessary to do this are derived from the real charge values.

To find the values of the third group of real charges, a special procedure is applied. A set of control points is chosen on the surface of electrodes. On the one hand, the potential at each of these points is known. The points are on the surface of the conductive electrode, which is connected to the power supply. On the other hand, the potential of each control point is the sum of partial potentials of all charges from the charge ensemble. The number of control points is equal to the number of charges of the third group. The charges of the first two groups are known. So, the values of the surface charges can be determined from a set of linear equations of the potential at the control points.

With this procedure the potential at the boundary of the integration region is calculated with high accuracy at each time step and the discharge dynamics can be described precisely, especially in the region next to the dielectric surface. Moreover, the knowledge of the total charge at the conductive electrode allows the conjunction of the discharge process in the discharge region with the current in the power supply circuit. The temporal change in the sum of these charges is just the current of the power supply (according to definition). The inclusion of the charges of the conductive electrodes in the model enables the simulation of the interaction of the power supply circuit with the discharge dynamics.

3.4. Electric field distribution

The initial field strength distribution above the dielectric surface is presented in figure 19. The tangential field strength component (along the dielectric surface) reaches its maximum in between the position of the electrodes. The normal field strength component (perpendicular to the dielectric surface) is positive at the location of the positive electrode (left one) and negative at the earthed one. This means electrons drift from the right to the left electrode.

To trigger the discharge, seed electrons are injected into the discharge region. Their initial distribution (a homogeneous layer on the conductive electrode or dielectric surface) does not affect the following discharge dynamics. The electrons drift towards the anode along the dielectric surface and cause a discharge current (figure 20). The discharge current is calculated straightforward as the change in charge on the conductive electrode (definition of current). There are two asymptotic approaches of initial conditions connected with the power supply circuit and with charges on the conductive electrode(s). The first one is characterized by an infinite bandwidth of the power supply, i.e. the electrode potential (voltage) remains constant. The second one is based on the assumption that the bandwidth is close to zero, i.e. the discharge is disconnected from the power supply and the value of charges on the electrode(s) is constant. The power supply current in figure 20 and the results in this section are obtained with the assumption of ‘constant voltage’, while the real circuit is in between both cases. The asymptotic approach (‘constant charge’ case) is also modelled. In this case, the

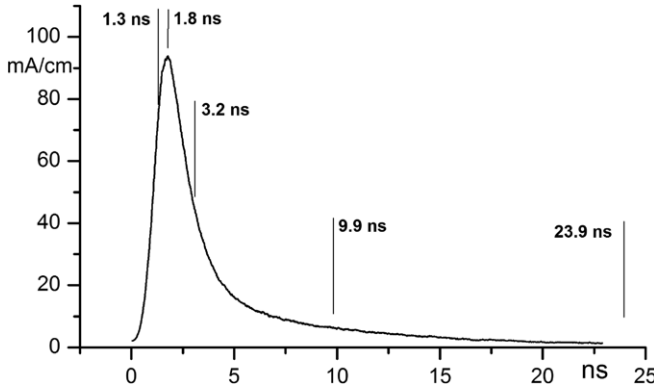


Figure 20. Discharge current of a CD channel.

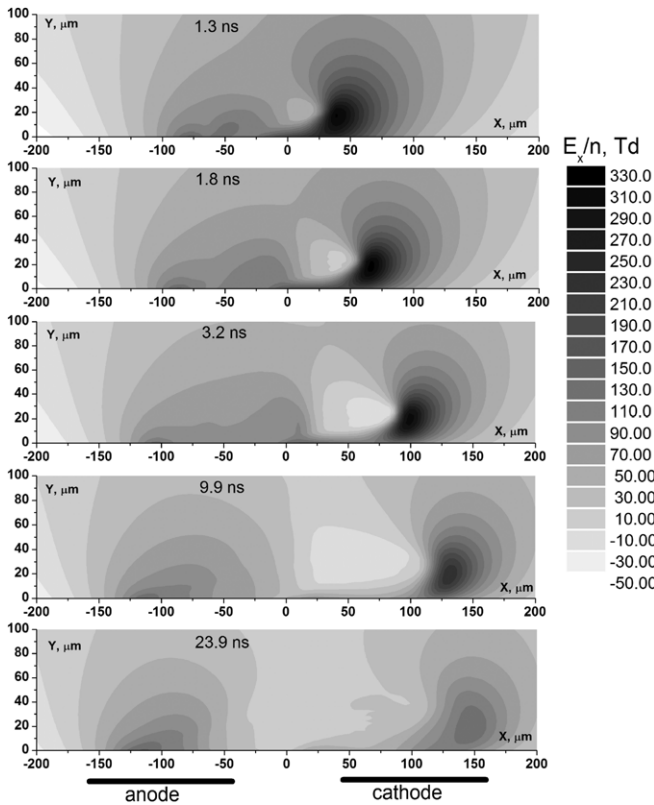


Figure 21. Distribution of the x -component of the field strength (for boundary conditions see section 3.2).

current amplitude, electron and ion densities, etc are 20–30% lower, while the main features are quantitatively the same.

The current shape in figure 20 consists of a steep rise and a comparably slow decrease. The amplitude of the discharge current is comparable to that of the microdischarge in the VD arrangement, while its duration is considerably shorter (compare figures 9, 11 and 20). The seed electrons multiply their number by collision processes. The electron number density rises and a field distortion (cathode-directed streamer) appears before the cathode (figure 21, 1.3 ns).

The amplitude of the field distortion is 1.5 times larger than the maximum of the initial field strength. In a few nanoseconds this maximum propagates along the cathode and passes a distance of 50–70 μm (figure 21). The propagation

velocity of the cathode-directed streamer nearly reaches the value of 10^7 cm s^{-1} (table 2), which is comparable to that in the VD case and with the electron drift velocity. The cathode-directed streamer propagates in the opposite direction of the electron flux.

A secondary maximum of the x -component of the field strength appears above the anode as well (figure 21, 1.3 ns). It belongs to the anode-directed streamer, which propagates in the direction of the electron flux (to the left-hand side). The velocity of the anode-directed streamer is about three times as low as the cathode-directed one (table 2). The thickness/width of both streamers is about 20–30 μm (figures 21 and 24). The initial field distribution smoothed during the propagation of the streamers (figure 22). A plateau of low field strength (with a level of 50–70 Td) appears in between the streamers in the range of about –40 and +40 μm (see figures 21 and 22), its length reaches a value of about 150–200 μm .

The y -component of the field strength has a pronounced minimum of field strength near the cathode, below the cathode-directed streamer (figure 22, right-hand side). Its amplitude reaches a level of about –900 Td. The parameters of this structure, e.g. the value of field strength and current density (100 – 200 A cm^{-2}), are not far from those of the cathode layer of normal glow discharges. The thickness of this structure (cathode layer) in the y -direction is 20 μm and its length in the x -direction 50–60 μm at 1.3 ns. This movable cathode layer appears behind the cathode-directed streamer and disappears after the coverage of a distance of 50–80 μm . With the streamer velocity given in table 2 this means that the layer disappears in less than 10 ns.

The decay of the cathode layer is caused by the accumulation of positive charges on the dielectric surface. This happens, on the one hand, due to the movement of positive charges from the discharge region (to a smaller fraction), but mainly due to the emission of secondary electrons. The latter process, initiated by photons and positive ions interacting with the dielectric surface, causes the emission of electrons leaving positive charges behind on the dielectric surface.

The electrons, which are emitted at the cathode side of the discharge region, move through the cathode streamer, the field strength plateau and finally reach the dielectric surface at the location of the anode. The y -component of the field strength becomes zero here (figure 22); however, electrons move farther and finally reach the far edge of the anode position during the extinction phase.

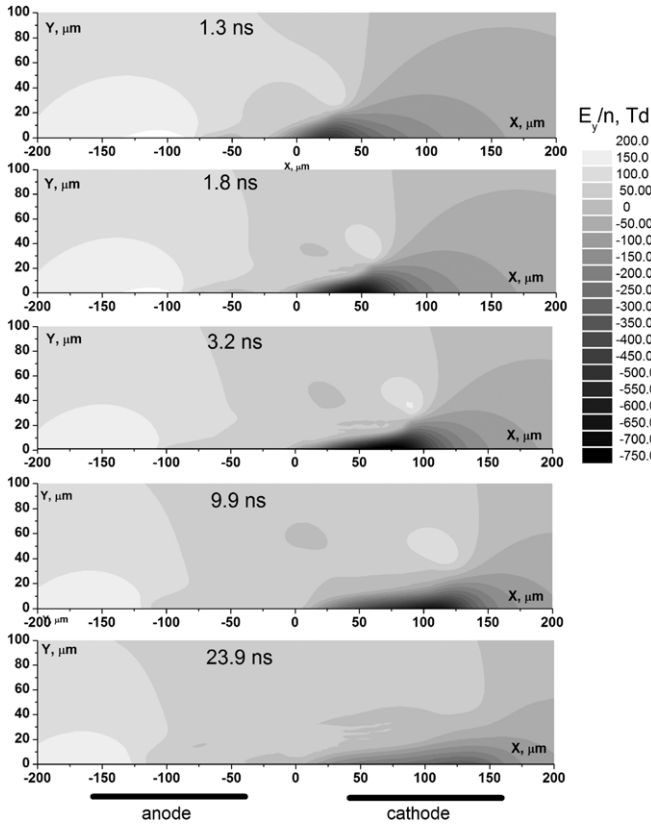
The duration of the streamer phase is about 5 ns under the given conditions. During the decay phase, which follows the streamer phase, the intensity of all discharge processes decreases due to a significant drop in the mean field strength. From this moment, ion movement determines the discharge behaviour and causes a further smoothing of the field strength distribution.

3.5. Dynamics of charged particles

A highly conductive channel with maximum electron densities up to 10^{14} cm^{-3} develops behind the streamers (figure 23) at the location of the field strength plateau. The conductive

Table 2. Parameters of the streamers in CD arrangement.

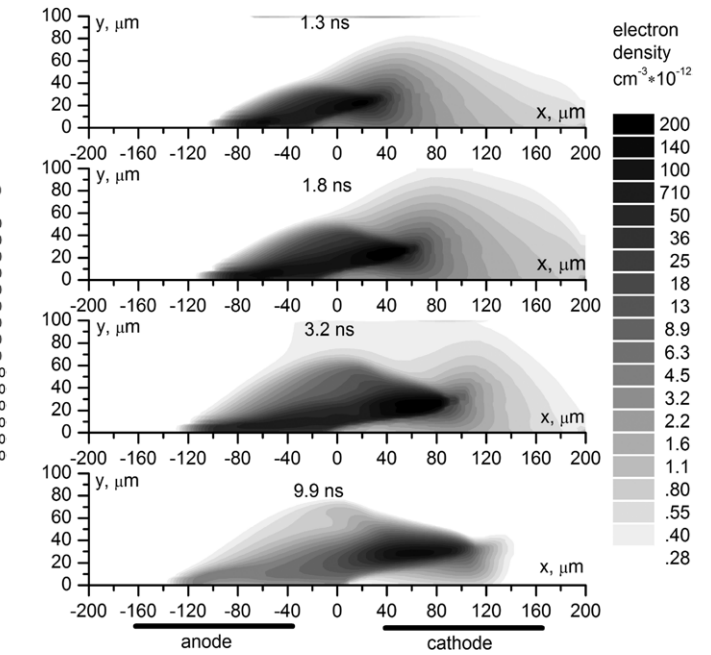
| | Time (ns): | 1.3 | 1.8 | 3.2 | 9.9 | 23.9 |
|---------------------------|---|-----|-----|-----|------|------|
| Cathode-directed streamer | Position (μm) | 40 | 70 | 100 | 130 | 150 |
| | Velocity/ 10^6 (cm s^{-1}) | — | 6.0 | 2.0 | 0.5 | 0.14 |
| Anode-directed streamer | Position (μm) | 80 | 90 | 100 | 110 | 115 |
| | Velocity/ 10^6 (cm s^{-1}) | — | 2.0 | 0.7 | 0.15 | 0.04 |

**Figure 22.** Distribution of the y-component of the field strength at different time steps.

channel develops from both sides of the plateau (figure 23). Near the cathode side the channel grows due to secondary electrons. They originate from photoemission, because they arise in front of the streamer (compare figure 21 with 23). The size of the cloud of secondary electrons decreases with the decay of the discharge process (compare 1.3 ns with 3.2 ns and especially 9.9 ns in figure 23). The anode-directed streamer receives electrons from the discharge channel. The length of the channel finally reaches a length of 200 μm and more; its height is about 20–30 μm .

The density of any kind of charged particles in the channel increases during the rise in the current pulse. Later on, the densities of positive and negative charges in the discharge region reach maximum values and then decrease continuously during the extinction phase.

The net charge in the channel is close to zero; the channel is quasi-neutral. In the cathode layer the net charge is positive as in glow discharges. Near the anode at the opposite side of the channel the total charge density is negative. That is why a region with zero net charge must be present in between

**Figure 23.** Electron density distribution during discharge development (for boundary conditions see section 3.2).

the charged regions with opposite polarity, which reduces the external field strength.

A kind of equilibrium between the densities of the charged particles and the mean field strength exists in the channel. The attachment rate and the movement of electrons balance the electron production rate. If the electron density drops at a certain location of the channel, the field strength rises immediately. This rise will increase the ionization rate and decrease the attachment processes so that the electron density will also increase and vice versa. This is the reason why the field strength does not drop to zero but is about 80–100 Td (in electronegative gases). This value of field strength is close to that given at the crossing point of the curves of the attachment and ionization coefficient over field strength.

The surface charge density increases continuously (figure 24). In the streamer phase electrons are mainly collected on the dielectric surface (in the region from -150 to $0 \mu\text{m}$ in figure 24). The surface charge density increases up to a certain level (60 – 70nC cm^{-2}), at which the normal field strength component becomes zero. Succeeding electrons move over the surface and reach the dielectric surface at a farther distance increasing the size of the charged spot (the region with zero y-component of the field strength in figure 22). During the extinction and ion phase, ions smooth the surface charge distribution and finally cause a more symmetric shape (figure 24).

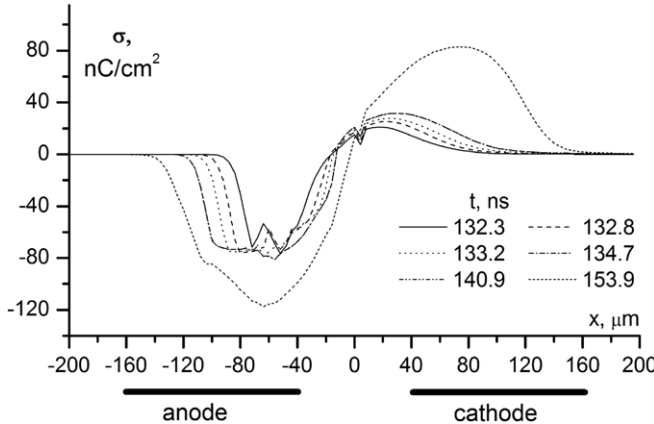


Figure 24. Distribution of surface charge density during discharge development.

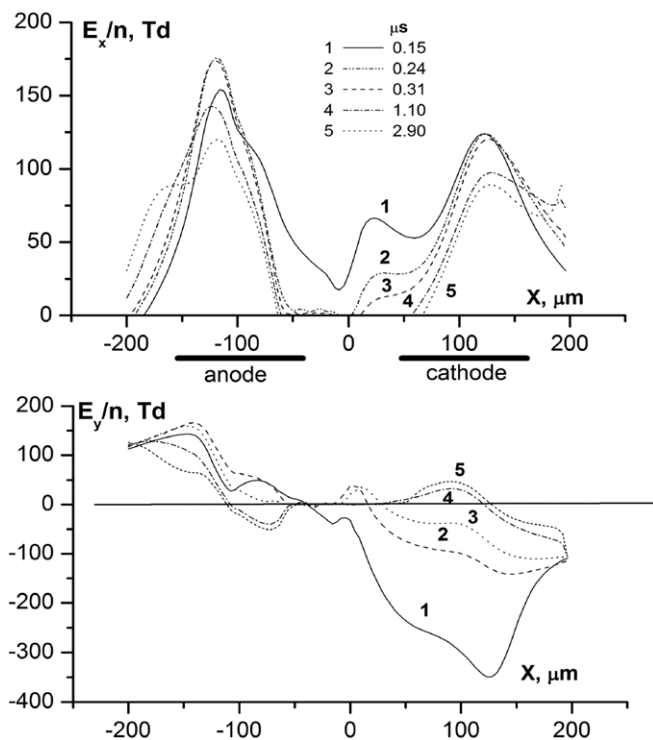


Figure 25. Distributions of the field strength components on the dielectric surface during the extinction phase of the discharge at different time steps.

From modelling it follows that secondary electrons from ion and photon impact on the surface are the promoters of discharge development. The exclusion of, e.g., the photo-processes retards the discharge development twice and the surface charge becomes more compact. The charge density does not exceed a level of $15\text{--}30 \text{nC cm}^{-2}$ in this case.

3.6. Extinction phase

After the end of the streamer phase the number density of electrons drops several orders of magnitude (extinction phase). The charge collected on the dielectric surface decreases the field strength in the discharge region. The excitation and dissociation processes cease. A considerable number of ions

of both polarities are left in the discharge region. The drift of these particles decreases the electric field furthermore and enlarges the surface charges. These charges determine the initial conditions of the next discharge pulse. Another effect of the ion drift is an additional energy loss, which reduces the overall efficiency of the excitation and dissociation processes.

The time duration of the extinction phase is less than $1 \mu\text{s}$ under the given boundary conditions. After this period the distribution of the surface charge density becomes practically symmetric (bipolar) and the charged region on the dielectric surface expands to the far edges of the location of the electrodes. Both components of the field strength on the surface become zero between the location of the electrodes, and the cathode layer disappears (figure 25). A field strength reduction takes place not only on the dielectric surface, but also in the gas region up to about $70\text{--}100 \mu\text{m}$ above the surface.

The ion drift ceases after about half a microsecond. Part of the ions have reached the dielectric surface, part of them are left in the discharge volume. The discharge volume is now practically neutral and the density of the ions of both polarities is about 10^{14} cm^{-3} . The ions cannot drift any longer because of the drastically reduced field strength. The main part of the ions is neutralized by recombination between 50 and 700 ns. After this period the discharge region becomes practically free of charged particles and the field strength is zero (the surface charges compensate the external voltage). If ignition conditions are reached again in the gas space, e.g. by voltage rise or polarity change, the next discharge pulse will occur.

3.7. Energy release in the discharge volume

Energy release starts with the current flow and practically stops when the charged particle density in the discharge region decreases significantly. The drift of electrons and ions determines the energy release. The energy release connected with the electron drift happens mainly during the current pulse. The drift of ions becomes important later on.

The energy density w can be described by the time integral of scalar multiplications of the local field strength with the drift velocity of all charged particles as follows:

$$w = e_0 \cdot \int \left(\sum |(\vec{E} \cdot \vec{v}_i)| \cdot n_i \right) dt \quad (4)$$

where e_0 is the elementary charge, and the other values are the same as in equations (1)–(3). Each kind of charged particle (electrons and ions of both polarities) contributes to the energy consumption.

First traces of energy release appear with the streamer development near the anode (left electrode in figure 26). A region with significant energy density is behind the cathode-directed streamer in the highly conductive channel, which grows and widens with the propagation of the streamer (compare figure 21 with 26). The maximum of the energy density is at the height $20 \mu\text{m}$ above the surface during this process. The mean value of energy density in the discharge channel is about 15 mJ cm^{-3} . After current maximum a second important region of energy release appears near the cathode (figure 26, $t = 9.9 \text{ ns}$).

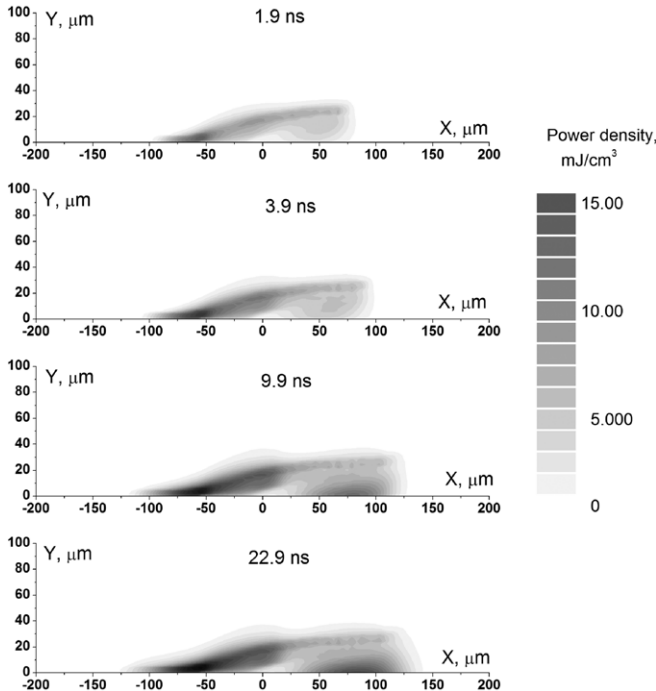


Figure 26. Distribution of the energy density in the discharge region at different time steps.

Part of the energy in the discharge region may be used for application purposes. For example, excitation of internal states of xenon is used in PDPs, dissociation of poisonous gases is applied for gas cleaning purposes and dissociation of molecular oxygen for ozone production. These processes occur during the streamer phase of the discharge, when the electron density is high. While the electron collisions last for a few nanoseconds, the subsequent processes like chemical reactions occur later on.

3.8. Lissajous figures

So far parameters of a single microdischarge have been considered. However, CDs consist of numerous tiny discharge channels on the dielectric surface. Some overall parameters of DBDs (averaged over the number of microdischarges/discharge current pulses which occur during voltage rise) can be derived from charge–voltage diagrams (Lissajous figures).

The dynamics of a single microdischarge in a CD arrangement is modelled two-dimensionally. In order to take into account the influence of preceding microdischarges on succeeding ones, the charge on the dielectric surface, which is left by the preceding ones, is included in the model. To realize this the channel number density and channel width taken from experiments are used to get the averaged surface charge density. With this procedure a set of simulations with consecutive discharge pulses is performed. The initial conditions for succeeding pulses are determined by the actual voltage value and the surface charge distribution resulting from preceding discharge pulses.

In figure 27 current pulses (from sets of microdischarges) are added to the displacement current and depicted together

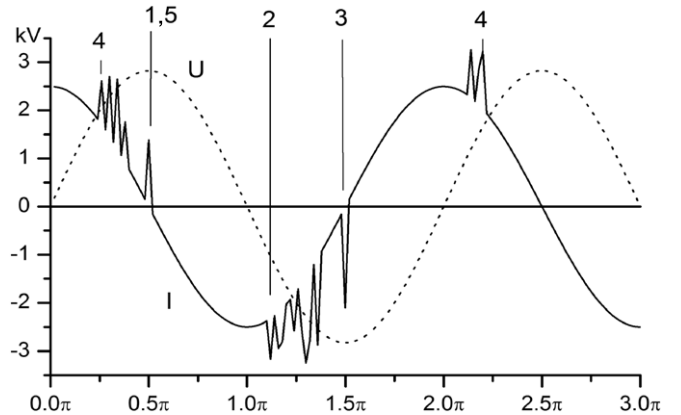


Figure 27. Current and voltage curves of a discharge in a CD arrangement (current per cm electrode length in arbitrary units).

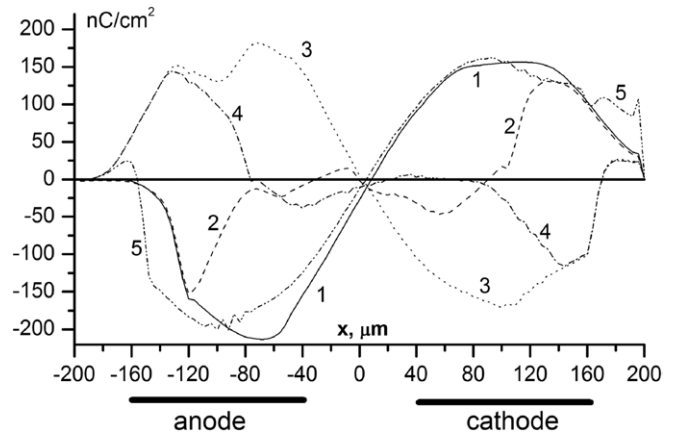


Figure 28. Distribution of the surface charge density after several current pulses (the time moments are marked in figure 27).

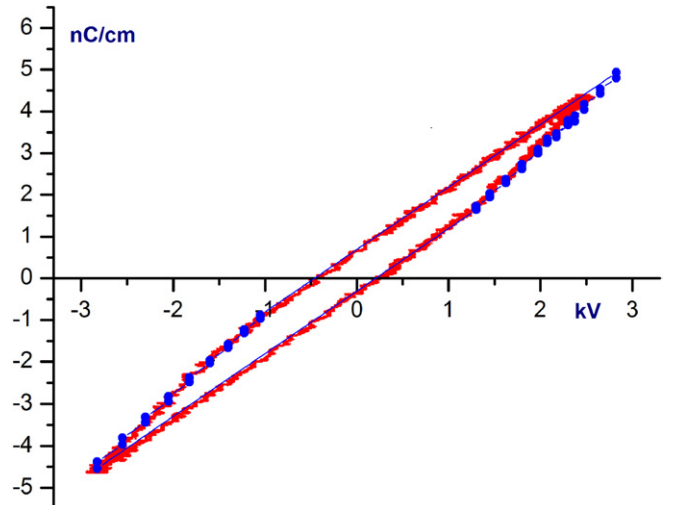


Figure 29. Simulated (dots) and experimental Lissajous figures.

with the voltage course. The resulting current appears in the external circuit.

The first current pulse occurs at the breakdown voltage (figure 27). Further pulses appear with voltage rise up to the voltage peak. During the second half-cycle of the applied voltage breakdown conditions are reached at a remarkably

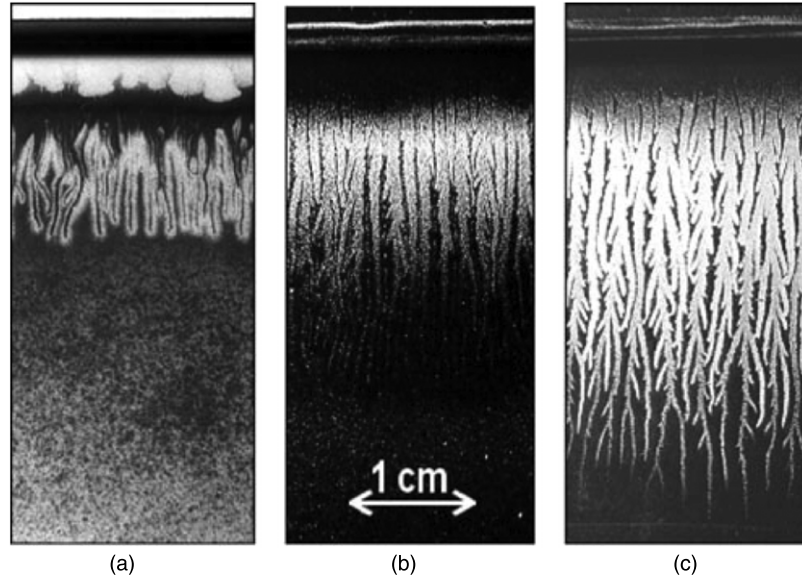


Figure 30. Dust figures of the surface discharge on dielectrics with different relative permittivities (anode: wire electrode on the top, relative permittivities: 9.8 (a), 4.8 (b) and 2.4 (c) [56]).

lower voltage level because of charge accumulation of opposite polarity on the dielectric surface.

Each current pulse changes the charge distribution on the dielectric surface. The distribution is bipolar; a positive charge is situated at the position of the actual cathode and a negative one at that of the anode (figure 28). The value of the surface charge changes and turns its sign together with the polarity of the applied voltage. After a period of the applied voltage the former distribution returns.

The simulated Lissajous figure in figure 29 is constructed based on the voltage–current curves in figure 28. The corresponding experimental one is also added. Both are in rather good agreement. The ignition voltage, which follows from modelling data, is in satisfactory agreement with the measured one. The deviation is smaller than 15%.

4. Surface barrier discharge

4.1. Some experimental findings of surface barrier discharges

In VD and CD arrangements the distance between the electrodes is fixed, i.e. the discharge region is limited in space. This limitation influences the duration and dynamics of the discharge process. In contrast, the DBD in SD arrangements is not influenced by this limitation. In general, these arrangements consist of a dielectric layer with an elongated high-voltage electrode on the surface (e.g. a thin wire) and an extended counter-electrode on the reverse side of the dielectric layer. These arrangements are asymmetrical ones with a conductive electrode on the surface and a dielectric counter-electrode (figure 1(b)).

The discharge develops along the conductive electrode on the dielectric surface ([53, 54], figure 30). It consists of distinct parallel discharge channels, which originate at the conductive electrode and terminate somewhere on the dielectric surface. The channels seem to appear simultaneously and develop

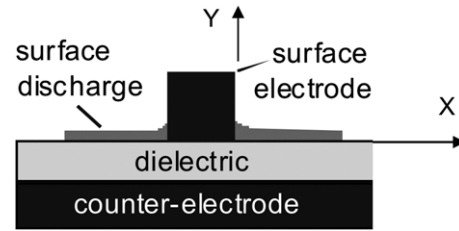


Figure 31. Sketch of the SD arrangement under investigation (cross-section).

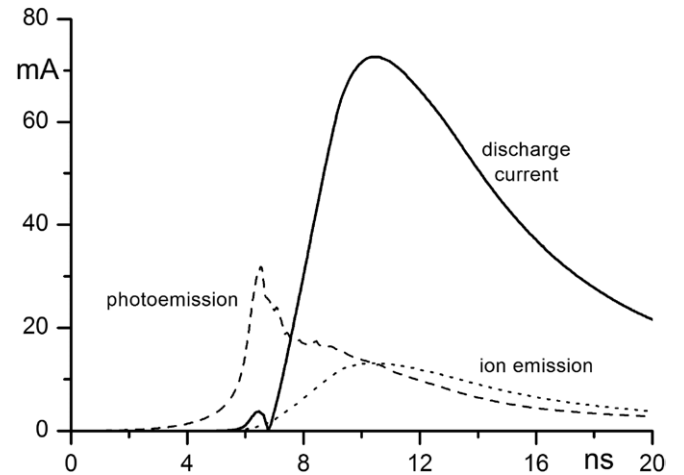


Figure 32. Currents in the SD arrangement at negative polarity of the surface electrode (discharge current in the power supply circuit, photoemission current from surfaces and current due to secondary electrons from ion impact).

independently from their neighbours. Preceding channels influence the succeeding ones by surface charges left on the dielectric surface.

The discharge patterns are comparable to those found in VD arrangements with a dielectric cathode (figure 3(b)).

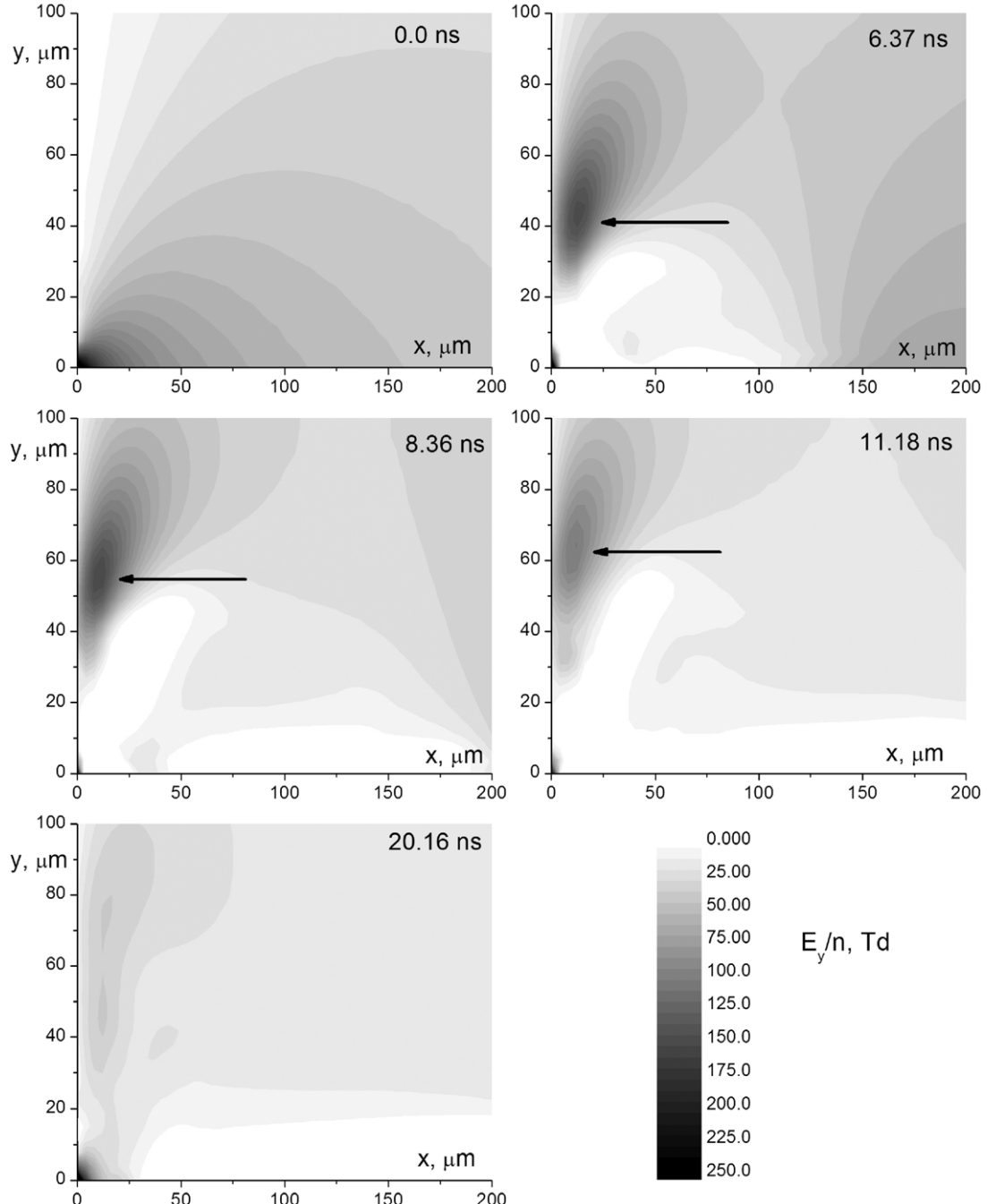


Figure 33. Distribution of the y -component of the field strength at different time steps (the arrows indicate the position of the cathode-directed streamer).

With rising voltage the area covered by the discharge channels grows. In contrast, in SD and VD arrangements the number of microdischarge channels grows with rising voltage (up to the peak voltage).

The absence of a certain discharge gap is the reason for the appearance of so-called backward discharges in figure 30 (in between the conductive electrode and the discharge channels). A backward discharge occurs during the decrease in the applied voltage when the field strength between the surface charge (near the conductive electrode) and the actual potential of the surface electrode reaches the breakdown value.

4.2. Simulation model

The mathematical model is based on the idea that the SD discharge consists of a set of parallel microdischarge channels, which propagate perpendicular to the conductive electrode on the dielectric surface (e.g. [16]). The physical model and its mathematical formalism are close to those applied for the description of CDs in section 3. They are improved and adapted to the SD arrangement. The charge dynamics is described by a set of continuity equations, which is solved in a 2D approach. The xy -plane crosses a microdischarge

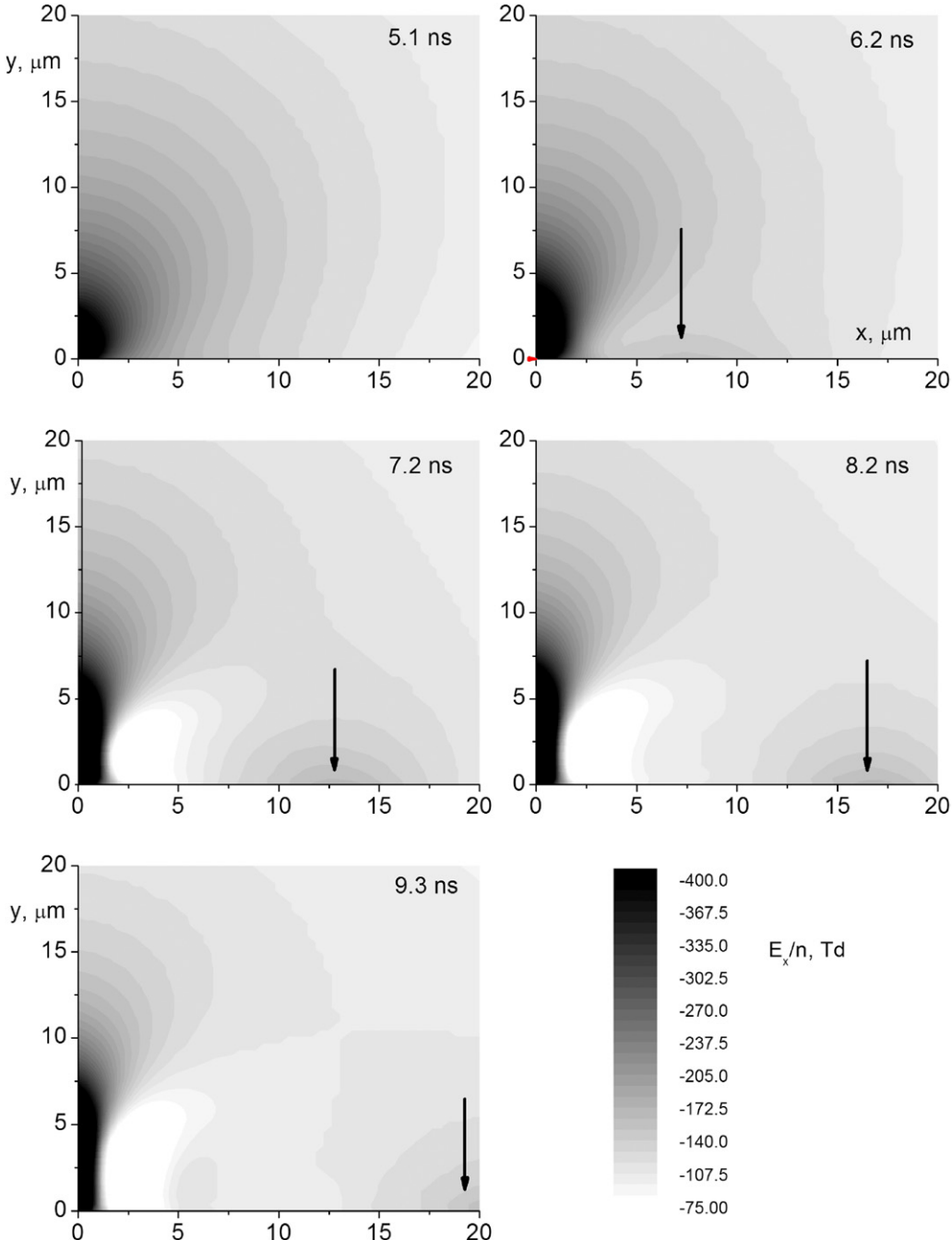


Figure 34. Distribution of the x -component of the field strength at different time steps (the arrows indicate the position of the anode-directed streamer).

channel along its length (figure 31). The x -axis is directed along a channel and the y -axis normal to the dielectric surface. The cross-section of the surface electrode is taken as $3 \times 3 \text{ mm}^2$; the thickness of the dielectric layer is 2 mm and the relative permittivity of the dielectric 8.4 (figure 31) close to experimental conditions [56].

The list of charged and neutral particles in oxygen and the chemical code are the same as those which have been used in the VD and CD models. The modelling is based on local thermodynamic equilibrium, i.e. the drift parameters and the rate constants of reactions with electrons are taken as a function of the local field strength.

The field strength distribution in the discharge region (xy -plane) is calculated with the differential grid method with a homogeneous grid and known potentials on the boundaries, which surround the integration region. Since the discharge develops on the dielectric surface, precise knowledge of the boundary conditions on the dielectric surface is essential. It is determined three-dimensionally, i.e. the width of the microdischarge channel is taken into account. In order to determine the boundary conditions precisely, three groups of real charges are considered as in the CD case, charges in the discharge volume (gas space), charges on the dielectric surface and charges on the conductive electrode. All charges are

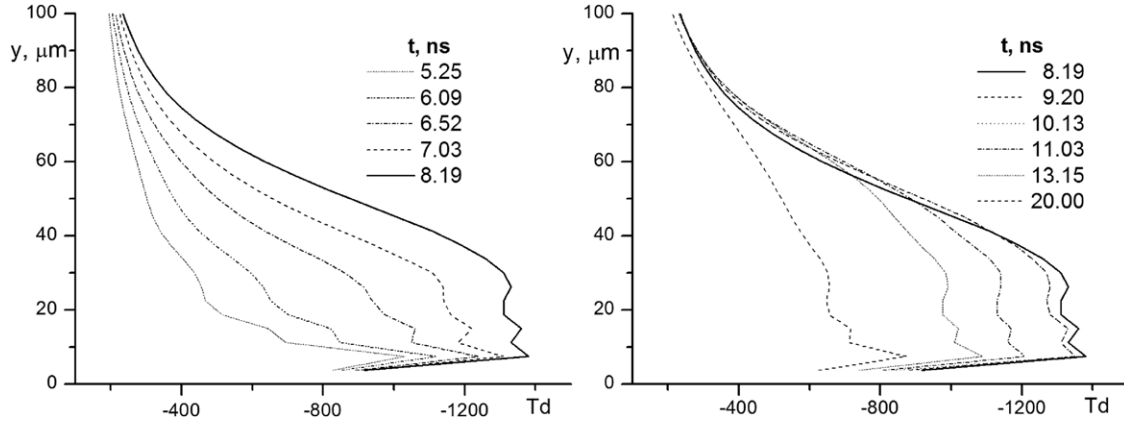


Figure 35. Distribution of the x -component of the field strength on the surface of the conductive electrode at $x = 0$ for different time steps and negative polarity of the surface electrode.

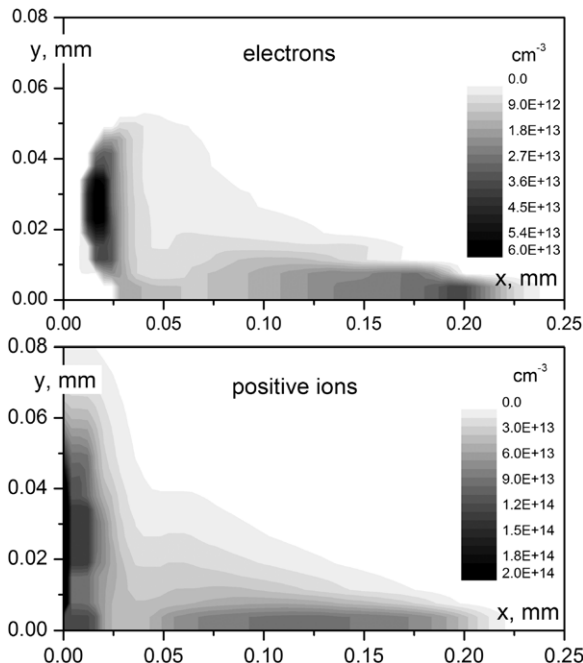


Figure 36. Particle densities in a channel of the SD at 8.36 ns (negative polarity of the surface electrode).

considered to have a certain length in the z -direction (along the conductive electrode length) with homogeneous charge distribution (line charges). The length is equal to the width of the microdischarge channel and is taken to be $100 \mu\text{m}$ (experimental result, figure 30, [56]).

For accurate determination of the boundary conditions, a precise solution of the Poisson equation is used as in the CD case. It is an analytical solution for a line charge within stacked dielectrics. The solution is the sum of the initial charge together with an infinite set of image charges, whose positions and values are given by the thickness of the dielectric layer and its permittivity. Each charge of the ensemble of real and image charges is mirrored at the conductive electrodes (surface and earthed electrodes). Finally, the potential at each point of the boundary of the integration region is the sum of partial potentials of each charge of the charge ensemble.

The values of the real charges in the discharge region and on the dielectric surface are obtained as a solution of the set

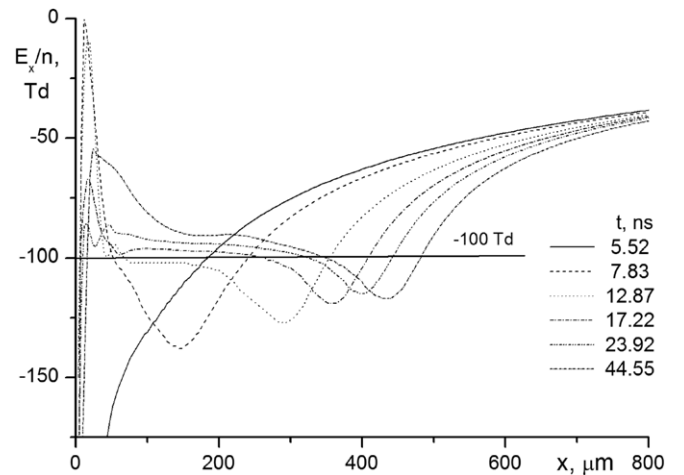


Figure 37. x -component of the field strength $23.2 \mu\text{m}$ above the dielectric surface of the SD arrangement.

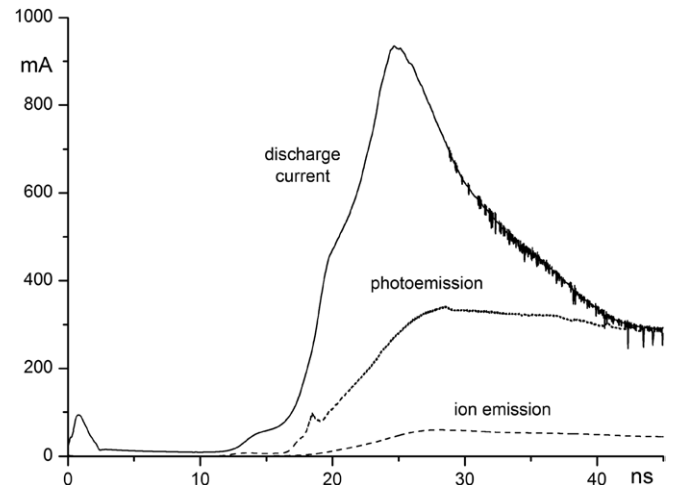


Figure 38. Currents in the SD arrangement at positive polarity of the surface electrode (discharge current in the power supply circuit, photoemission current from surfaces and current due to secondary electrons from ion impact).

of continuity equations at each time step. The values of the corresponding image charges are derived from those of the real charges (as described in the previous section). The values of the charges on the conductive surface of the high-voltage

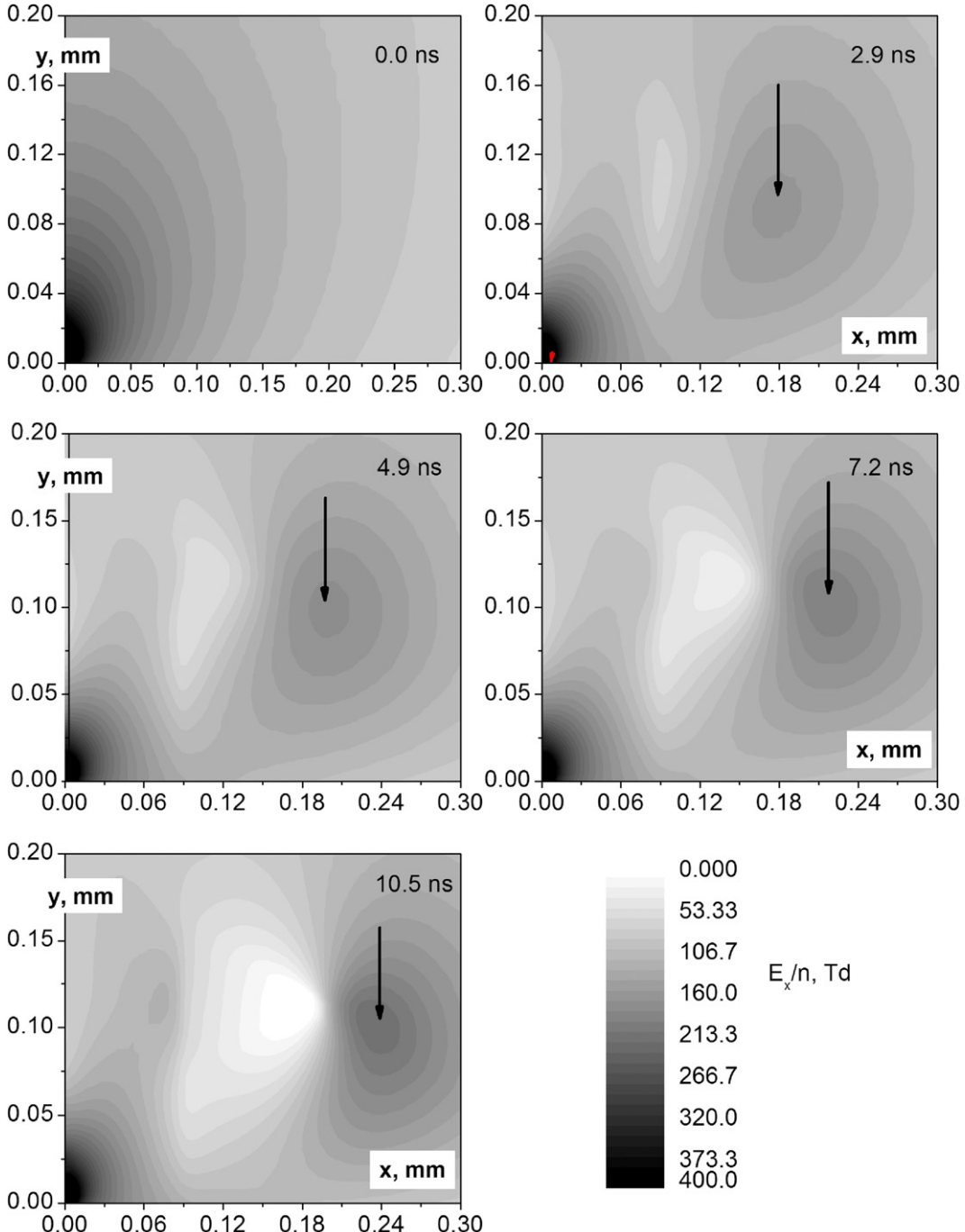


Figure 39. Distribution of the x -component of the field strength in the discharge region near the surface electrode at different time steps (the arrows indicate the position of the cathode-directed streamer).

electrode are determined with the algorithm, described in the previous section (control points and known potential of the conductive electrode).

With known charge values at the conductive electrode the current of the power supply circuit can be determined. The temporal change in the total charge of the high-voltage electrode is the current of the power supply according to the definition. Moreover, the inclusion of the charge of the conductive electrode in the model together with discharge process allows the determination of the influence of the power supply circuit on the discharge dynamics.

The polarity of the surface (conductive) electrode determines the discharge dynamics. The dynamics with negative polarity is rather different from that with positive polarity. That is why both cases are considered separately.

4.3. Discharge dynamics at negative polarity of the surface electrode

The discharge process starts at the corner of the surface electrode and the dielectric surface at breakdown voltage (Paschen minimum condition). From the very beginning

electrons collide with heavy particles, cause electron multiplication and a photon flux to the surfaces. The photon flux generates secondary electrons from the surfaces and so on. This feedback supports a permanent acceleration of the breakdown process. Without photoemission the discharge development would be too slow to be comparable to experimental data.

The discharge current becomes significant several nanoseconds after electron injection, when the charge density has reached a certain level (figure 32). The photoemission current is a precursor of the discharge current in the external circuit. The continuous growth of photoemission current causes a permanent rise in the electron density near the cathode. Simultaneously, the field strength distribution near the conductive cathode is rearranged (figures 33 and 34). Two field distortions are observed in the discharge region, one moves along the conductive electrode (figure 33) and the second one along the dielectric electrode (figure 34). They are named cathode- and anode-directed streamers, like the terminology used for streamers in VD arrangements [21–23].

Both streamers appear simultaneously with the photoemission current (figures 32–34). The cathode-directed streamer moves along the conductive electrode (figure 33, arrows). Its velocity decreases quickly from $1.2 \times 10^6 \text{ cm s}^{-1}$ to zero and then the streamer disappears. The anode-directed streamer appears simultaneously with the cathode-directed one; its position is between $x = 175$ and $200 \mu\text{m}$ at 6.37 ns and propagates along the dielectric surface (figure 34, arrows).

During streamer propagation the following processes can be highlighted:

- (i) the x -component of the field strength in the discharge region is pressed to the surface electrode (formation of cathode layer, figure 34),
- (ii) the cathode layer expands in the y -direction due to the propagation of the cathode-directed streamer (figure 33) and
- (iii) the field strength in the cathode layer is nearly constant (about 1300 Td , figure 35).

The cathode layer hardly changes its size after 8 ns (figure 35), when the cathode-directed streamer does not propagate any longer, i.e. the maximum size of the cathode layer is reached at about current maximum (see figures 35, 36 and 32). This phenomenon is well known for normal glow discharges. The value of the discharge current is proportional to the size of the cathode layer. This is true for DBDs in VD arrangements as well (figures 9–12, [26]).

As described in section 2 in VD arrangements the appearance and propagation of field strength maximum (streamer) along the cathode surface are found experimentally [13–17, 21–23]. A thin bright layer appears near the cathode in the gas gap and propagates along the cathode surface. The thickness of the layer and its propagation velocity found by experiments [16, 21–23] are in good agreement with the corresponding modelling results for VD [26] and SD arrangements as well (figure 34).

The properties of the cathode layer in SD arrangements are not far from those of normal glow discharges. First of all, the

field strength in the cathode layer is constant and its maximum value is 1300 Td (figure 35).

After current maximum the field strength in the cathode layer decreases permanently. Simultaneously, the role of photoemission decreases (figure 32). The charged particles in the cathode layer form a dipole with the maximum of the positive ion density at the surface of the cathode and the maximum of the electron density at a distance of about $20 \mu\text{m}$ from this surface in the discharge region (figure 36).

The maximum value of field strength in the anode-directed streamer (on the dielectric surface) is lower than that of the cathode-directed streamer (figures 33 and 37). The photoemission process at the dielectric anode does not play any role. The electrons, which are released from the dielectric surface by photoemission, return immediately back to the surface due to the field configuration. The only source of electrons which reach the streamer is the cathode layer. The electrons from the cathode layer do not increase their number density significantly during their movement from the cathode layer to the streamer (figure 36). The mean field strength in the channel is close to 100 Td (figure 37). This value is determined by the equilibrium between the rates of electron attachment and electron multiplication. Because of the equilibrium the effective multiplication coefficient is close to zero. Thus, the anode-directed streamer is a non-self-sustaining phenomenon. Electrons from the microdischarge channel support its propagation. The size (width and height) of the streamer is in the order of $30\text{--}50 \mu\text{m}$ and its velocity is about $3 \times 10^6 \text{ cm s}^{-1}$ (figures 35 and 37).

The anode-directed streamer leaves a conductive channel. The channel is characterized by a comparatively high electron density ($2 \times 10^{13} \text{ cm}^{-3}$, figure 36) and equilibrium field strength of about 100 Td (figure 37). The same value was also found by modelling the DBD in a VD arrangement [26], and is in good agreement with experimental ones [15]. It is practically constant along the channel (figure 37) and results from the equilibrium between the rates of electron multiplication and electron attachment processes, which happen just at this level of field strength. The field strength is high enough to generate excited particles and radicals effectively.

4.4. Discharge dynamics at positive polarity of the surface electrode

At positive polarity of the surface electrode the currents rise almost simultaneously up to the peak current (figure 38, compare with figure 32). The time lag between the injection of seed electrons (at $t = 0$) and the appearance of a considerable discharge current is larger than that at the opposite polarity.

From the very beginning of the discharge a field distortion near the anode appears; at 2.9 ns a weak cathode-directed streamer is already detectable in figure 39. However, at this moment the discharge current in the external circuit is still practically zero (figure 38), i.e. the reconfiguration of the field distribution does not cause any significant charge transfer in the power supply circuit.

The value of field strength in the cathode-directed streamer grows permanently and a remarkable discharge current can be

detected in the external circuit at about 12 ns. At this time the current reaches a value of about 80 mA (the peak current value of the opposite polarity) and remains at a moderate value for some nanoseconds (14–17 ns in figure 38) before a further rise occurs at about 17 ns.

The maximum current value is reached at about 24 ns. It is an order of magnitude larger than that at negative polarity (figures 32 and 38). Simultaneously, the field strength in the cathode-directed streamer also reaches its maximum, which is about 600 Td (figure 40). The corresponding value at negative polarity of the surface electrode is only about 186 Td (figure 33). There is another difference related to polarity; starting from 16 ns the field strength behind the streamer (in the channel) decreases to zero (figure 40).

The cathode-directed streamer moves 50–125 μm above the dielectric surface (figure 39). Below the streamer, next to the dielectric surface, an additional field strength maximum (in the y -direction) appears (figure 41). It exceeds a value of 1000 Td, which is comparable to that of the cathode layer at negative polarity (figure 35).

At negative polarity of the surface electrode the cathode layer is fixed near the surface of the cathode. At positive polarity, however, the cathode layer propagates along the surface of the dielectric together with the cathode-directed streamer (figure 41). The cathode layer appears just below the streamer and fades out at a distance of about 0.5 mm behind the streamer (figure 41). The size of the cathode layer at positive polarity is 6–8 times larger than that at the opposite polarity. Accordingly, the discharge current at positive polarity is also 6–8 times larger (figures 32 and 38).

The moveable cathode layer disappears within about 5 ns (with respect to the streamer velocity) due to the permanent growth of the surface charge density, as shown in figure 41. The growth of the surface charge density results, on the one hand, from the flux of positive ions from the discharge volume to the dielectric surface and on the other hand from photoemission. Each electron emitted from the surface leaves a positive charge.

Photoemission is essential for cathode streamer development and streamer propagation along the dielectric surface. The main source of photons is at the centre of the streamer (above the surface). Photons reaching the dielectric surface in front of the streamer release electrons from the dielectric. These electrons move upwards, multiply and reach their maximum density in the streamer. Electron collisions not only multiply the electron number but generate new photons as well. They reach the dielectric surface and so on: it is a positive feedback. This feedback supports the existence and propagation of the cathode-directed streamer along the dielectric surface.

At positive polarity of the surface electrode the cathode-directed streamer, which propagates along the dielectric cathode, is a self-sustaining phenomenon and does not need any additional electron source for its development and expansion. Moreover, the streamer is a powerful source of electrons, which is much more effective than the cathode layer at negative polarity. Because of the rather high electron density behind the streamer ($2 \times 10^{14} \text{ cm}^{-3}$, figure 43(c)) the field strength in the discharge channel is close to zero (figures 40, 41 and 43) in contrast to the opposite polarity of the surface electrode.

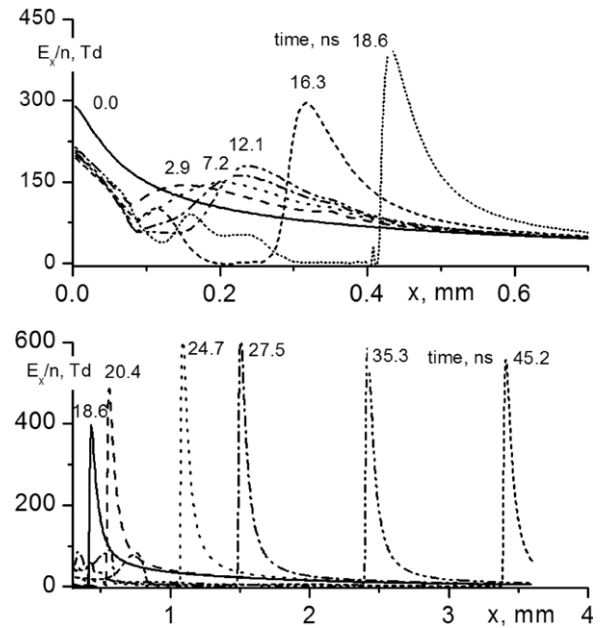


Figure 40. Temporal development of the cathode-directed streamer (x -component of the field strength) 41.2 μm above the dielectric surface at positive polarity of the surface electrode.

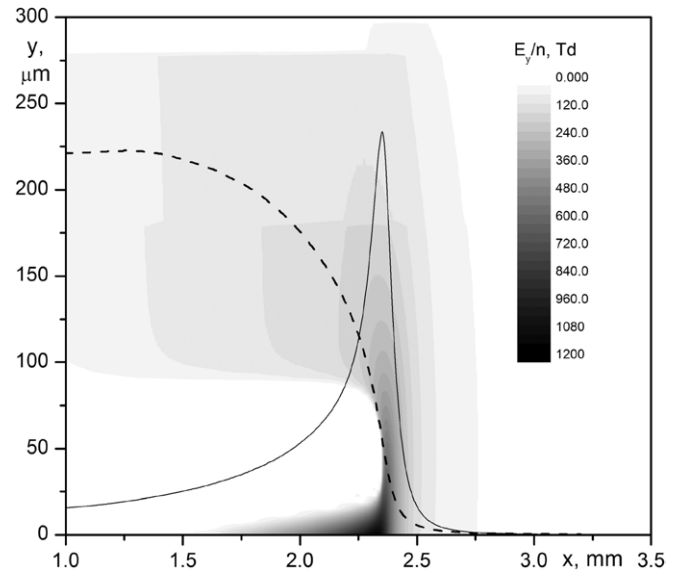


Figure 41. y -component of the electric field strength around the cathode-directed streamer at 35.25 ns and positive polarity of the surface electrode (grey shaded) and the profiles of the photoemission current density (solid curve) and surface charge density (dashed curve) in relative units.

4.5. Microdischarge channel and surface charge density

As described before, streamer propagation along the dielectric surface, followed by a conductive channel, takes place at both polarities of the surface electrode (figures 42 and 43). However, the feature of the streamer and the properties of the succeeding channel depend on polarity. At negative polarity of the surface electrode the value of the x -component of the field strength within the channel (along the dielectric surface) is about 100 Td (figure 42(b)) and at the opposite polarity it is close to zero (figure 43(b)).

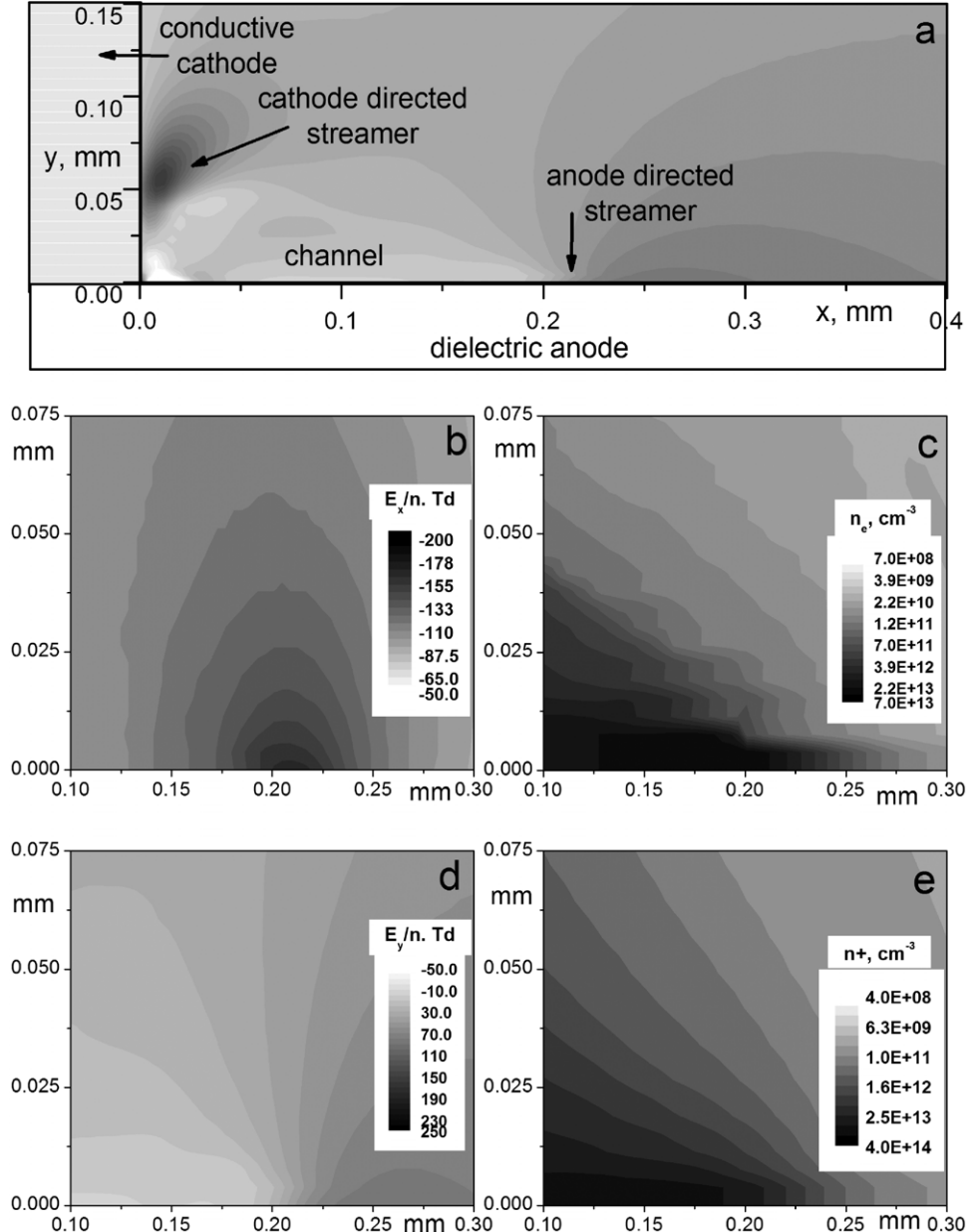


Figure 42. Calculated distributions of an SD with negative polarity of the surface electrode at 8.4 ns, (a) overview of the field strength distribution (y-component) within the discharge region, (b) x-component of the field strength, (c) electron density, (d) y-component of the field strength and (e) positive ion density.

The y-component of the field strength (perpendicular to the dielectric surface) is close to zero below the microdischarge channel for both polarities (e.g. figure 42). However, it is rather high below the streamer at positive polarity (higher than 1300 Td, figure 41). It decreases rapidly in the y-direction and becomes zero in the streamer and changes its sign above the streamer. As a result, electrons in front of, below and above the streamer move to the streamer (figures 43(c) and (d)). At negative polarity the maximum of the y-component of the field strength does not exceed a value of 100 Td (in front of the anode-directed streamer) and the sign of the y-component does not change within the discharge region (figure 42(d)), i.e. electrons move directly towards the dielectric surface.

As a result of streamer propagation and channel development, surface charges appear on the dielectric

(figures 44 and 45) and the y-component of the field strength near the surface decreases to zero. The streamers of both types initiate this charging process. Very soon the surface charge density reaches its saturation level of about 25–30 nC cm⁻². This saturation value is nearly identical for both polarities (figures 44 and 45).

At positive polarity of the surface electrode the high-conductive channel on the dielectric surface, which appears behind the streamer head, is practically quasi-neutral (figure 46). The term quasi-neutral means that the total charge in the conductive channel is close to zero. However, the whole discharge region (at 22 ns) is in general positively or negatively charged depending on polarity. This happens because some charge carriers leave the discharge region via the surface electrode. That is why the total charge differs locally from

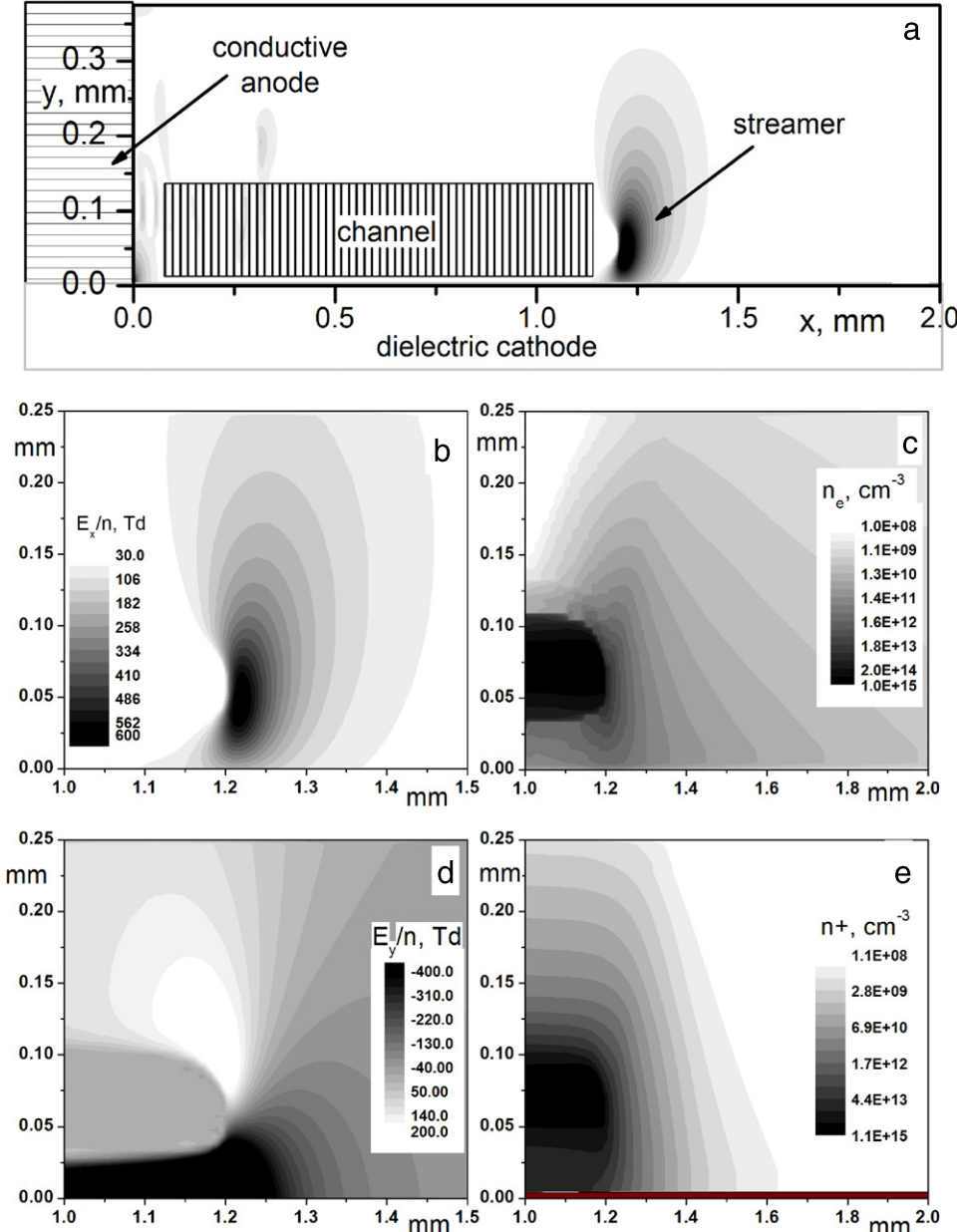


Figure 43. Calculated distributions of an SD with positive polarity of the surface electrode at 25.5 ns, (a) overview of the field strength distribution (x -component) within the discharge region, (b) x -component of the field strength, (c) electron density, (d) y -component of the field strength and (e) positive ion density.

zero and the distribution of the total charge is more complex (figure 46, logarithmic scale).

At this polarity the charge density distribution is determined by the special field configuration in front of the cathode-directed streamer. Electrons from any direction drift to the streamer head along the current lines. Finally, the streamer head absorbs all electrons and direct them to the channel in a region where the charge carrier density reaches a level of 10^{15} cm^{-3} and more (figure 46, $y = 15\text{--}110 \mu\text{m}$).

The distribution of electron density is narrower than that of the positive ions. The width of the ion density distribution is determined by the width of the electron density distribution *in front of* the streamer. In this region, positive ions arise from electron collisions. In the nanosecond range the ions practically do not move because of their low mobility and

maintain their distribution, which differs from that of the electrons (figure 46).

In contrast to the positive polarity, the channel, which is produced by the anode-directed streamer, is situated directly on the dielectric surface at negative polarity of the surface electrode (figures 36 and 43). The channel originates from the cathode layer (figure 36). Its length is smaller than that at the opposite polarity. The highest positive ion density in the cathode layer is about $5 \times 10^{14} \text{ cm}^{-3}$ and in the channel about $3 \times 10^{13} \text{ cm}^{-3}$ (figure 36), i.e. at least an order of magnitude smaller than that at the opposite polarity. The highest electron density in the channel is 10^{14} cm^{-3} . The discharge region altogether is negatively charged, because positive ions leave the discharge region through the conductive cathode. The (final) length of the (comparatively) high-conductive channels

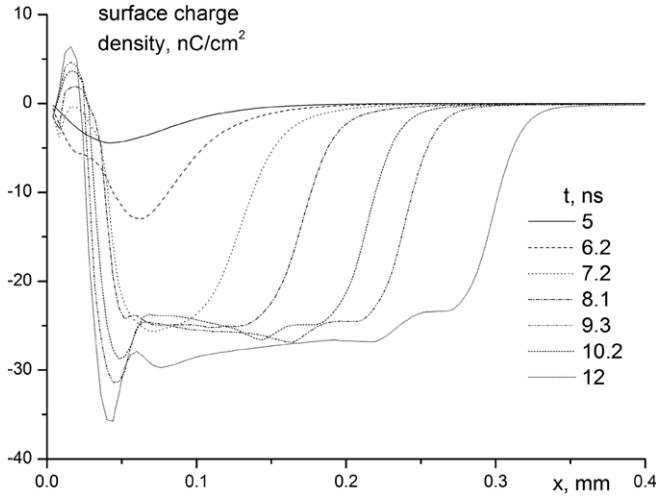


Figure 44. Surface charge density on the dielectric surface at negative polarity of the surface electrode (SD arrangement).

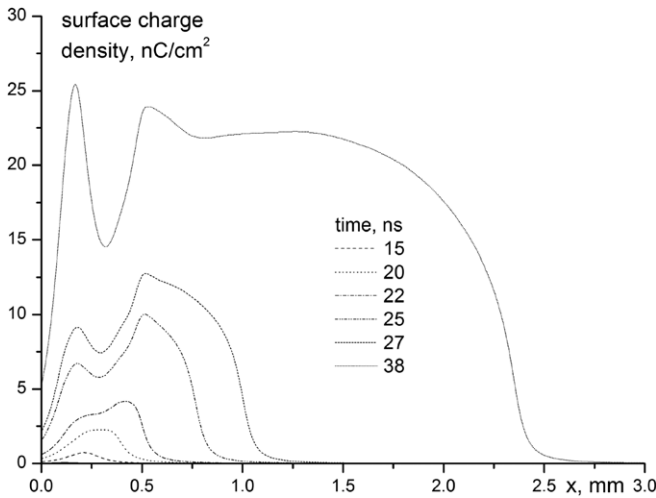


Figure 45. Surface charge density on the dielectric surface at positive polarity of the surface electrode (SD arrangement).

(microdischarges) on the dielectric surface, which is found by simulation, is in satisfactory agreement with experimental data for both polarities (table 3). At positive polarity it is five times longer than at the negative one.

4.6. Discharge energy

The energy transfer from the electric field to the gas particles occurs in the whole discharge region, i.e. in the streamers, microdischarge channel and cathode layer. As has been found by modelling, the energy density of a microdischarge at both polarities does not exceed the level of $50\text{--}70 \text{ mJ cm}^{-3}$. This means the local temperature jump in the gas due to a microdischarge is smaller than 80 K taking into account the specific heat capacity of oxygen.

There is no significant energy release in the anode-directed streamer at negative polarity of the surface electrode. While the field strength in the streamer is slightly higher than that in the channel, the streamer size is small compared with the channel length. The main energy release occurs in the cathode layer and channel (figure 47). Approximately, 20–30% of the energy

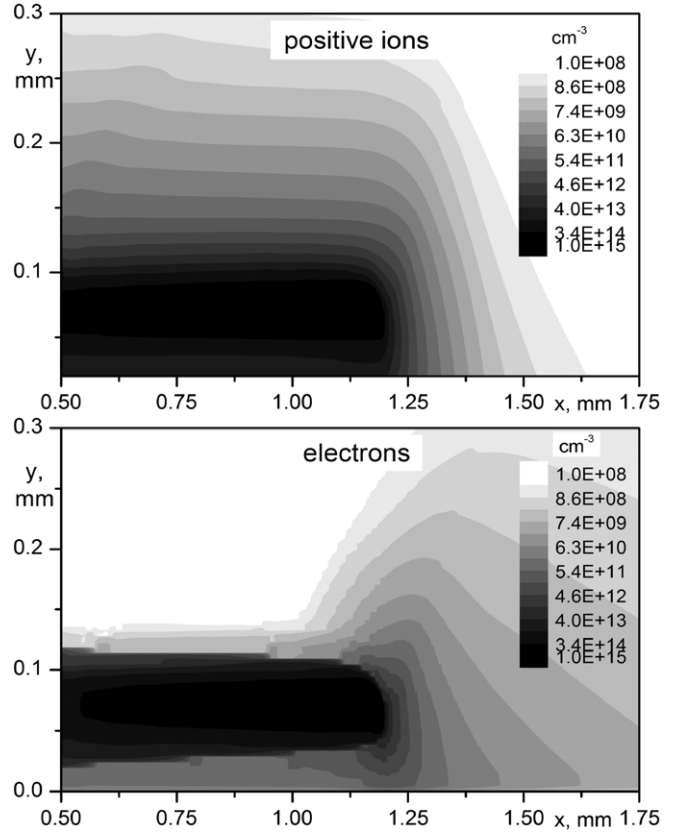


Figure 46. Particle densities in a microdischarge channel at 22 ns (SD arrangement, positive polarity of the surface electrode, logarithmic scale).

Table 3. Length of the microdischarge channel for both polarities of the surface electrode for the conditions given in [57].

| Polarity | Simulation (length in mm) | Experiment [57] (length in mm) |
|----------|------------------------------|-----------------------------------|
| Negative | 0.8 | 1.0 |
| Positive | 4.0 | 5.0 |

release happens in the cathode layer. The energy density in the cathode layer is an order of magnitude higher than that in the channel; however, the thickness of the cathode layer is small compared with the channel length. Thus, the temperature jump in the main part of the discharge region is only a few degrees on average (4–6 K). In a very narrow region next to the electrode, the temperature jump may reach 60–80 K. This energy release can effectively be transferred to a cooling system, because it takes place just on the electrode surface.

In contrast to the negative polarity of the surface electrode, the main energy release at positive polarity takes place in the cathode-directed streamer (figure 48). There is no significant change in the energy density behind the streamer in the discharge channel, because the effective field strength is almost zero in the channel. Close to the (conductive) anode surface some energy release is observed, which is connected with the field strength growth in this region (figure 48). The microdischarge channel is not neutral here because positive ions leave the discharge region through the conductive surface. The field strength rises and this is why approximately 50% of

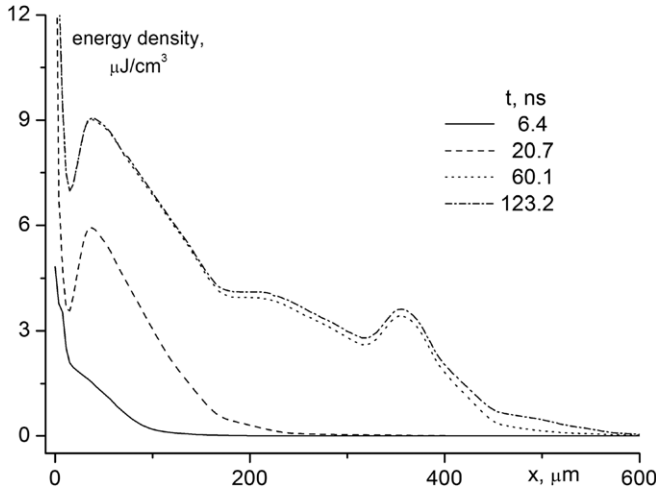


Figure 47. Temporal development of the energy density distribution of an SD with negative polarity of the surface electrode at a height of 45 μm above the dielectric surface.

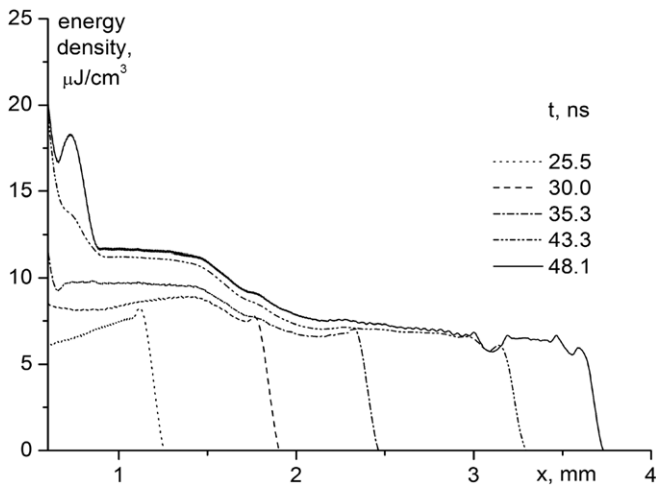


Figure 48. Temporal development of the energy density distribution of an SD with positive polarity of the surface electrode at a height of 64.8 μm above the dielectric surface.

the energy is released at a distance of up to about 0.75 mm from the conductive anode. The remaining 50% of energy is dissipated in the cathode-directed streamer and only a small part in the channel with a length of more than 3 mm. The average temperature jump in the discharge channel does not exceed 10 K.

In table 4 simulation results of some parameters characterizing the surface discharge properties are summarized for the boundary conditions under consideration.

5. Discussion and results

5.1. Methodological remarks

In general, the theoretical description of a physical phenomenon emerges from simple models to more sophisticated ones. This line of development is driven by the comparison of theory with measurement on the one hand, and by the desire to pass from a qualitative to a more and more accurate quantitative

description on the other hand. In the case of DBD modelling the expected accuracy of the numerical approach has special importance because the main part of the results is currently not accessible by experiments.

In order to model the discharge development the following numerical procedures must be developed, a routine, which describes the time-dependent movement of charged and neutral particles, and a routine to solve the Poisson equation with proper boundary conditions.

The procedure to describe particle movement is well developed. There exist several approaches and discussions on, e.g., fluid, Monte Carlo, particle-in-cell and hybrid models. The limitations of all these methods are well known. The results of these approaches differ, but not very significantly. The differences are not qualitative. If a special behaviour or effect is detected by a certain approach, the same appears by applying the others, except in cases where the effect is based on non-local behaviour, e.g. the negative glow of glow discharges. The discharge characteristics such as breakdown voltage, streamer velocity, extension of the discharge and some application properties of the plasma source are predicted by all mentioned methods with reasonable accuracy. The deviations are only in the order of percentages (e.g. [30, 36, 37, 58, 59, 60]).

An approximate description of charged particle transport is a first source of possible errors in modelling results [52]. In [52] a second source is mentioned: the accuracy of data used in the simulations such as cross-sections and transport coefficients. There exists an additional third source of possible errors: the value of field strength. The multiplication coefficients of electrons depend on field strength exponentially. Hence, the computational accuracy of the field strength value has at least the same importance as the choice of the particle transport method. The accuracy is of special importance for modelling of DBDs, where numerous processes take place on and near the surface of the dielectric. The accuracy of the field profile near the dielectric surface is determined by the accuracy of the boundary conditions. These are defined by the continuous change in the potential along a path from the gas space into the dielectric and the relations for the normal and parallel electric field strength components of the dielectric surface. Usually, the Poisson equation solver takes into account the continuous change in potential and the relation for the normal field strength component. The neglect of the relation for the parallel component results in a certain error of the field strength value up to a distance of several discretization cells in the gas region above the dielectric surface.

In order to obtain exact boundary conditions at the dielectric surface, the image charge method is applied [52]. The introduction of image charges, which are based on real ones (in the gas region and on the metallic and dielectric electrodes), allows satisfying the quoted boundary relations automatically. The potential along any boundary, in particular on the dielectric surface at each time step, is determined by the charge ensemble of real and image charges precisely. It is a Dirichlet task with known potential on the boundary (or boundaries). By solving this task with any suitable method, the field distribution in the integration region and close to the dielectric surface can be found.

Table 4. Characteristic values of surface discharges for both polarities of the surface electrode.

| Parameters | Polarity | |
|---|------------------------------------|------------------------------------|
| | Negative | Positive |
| Cathode material | Conductive | Dielectric |
| Discharge structure near the cathode | Cathode layer | Moveable cathode layer |
| Width of the positive charge layer near the cathode | 20 μm | 100 μm |
| Length of the high-conductive region near the cathode ^a | 40–60 μm | 4.0 mm |
| Length of the high-conductive region near the anode ^b | 0.5 mm | 80 μm |
| Maximum surface charge density (saturation level) | –25 nC cm ^{–2} | 25 nC cm ^{–2} |
| Maximum field strength next to the cathode (normal component) | 1400 Td | 1400 Td |
| Maximum field strength next to the cathode (x -component, streamer head) | 200 Td | 600 Td |
| Maximum electron density in the microdischarge channel | $3 \times 10^{13} \text{ cm}^{-3}$ | $1 \times 10^{15} \text{ cm}^{-3}$ |
| Maximum positive ion density in the microdischarge channel | $8 \times 10^{13} \text{ cm}^{-3}$ | $1 \times 10^{15} \text{ cm}^{-3}$ |
| Maximum electron density in the cathode layer | $6 \times 10^{13} \text{ cm}^{-3}$ | $1 \times 10^{15} \text{ cm}^{-3}$ |
| Maximum positive ion density in the cathode layer | $3 \times 10^{14} \text{ cm}^{-3}$ | $1 \times 10^{15} \text{ cm}^{-3}$ |

^a Negative polarity—thickness of the cathode layer; positive polarity—length of the microdischarge channel.

^b Negative polarity—length of the microdischarge channel; positive polarity—height of the microdischarge channel above the dielectric surface.

This approach for the field calculation obviously has advantages.

- (i) In the frame of this approach it is possible to calculate the DBD current straightforwardly and precisely, because the accurate distribution of the surface charges on the conductive electrodes is known at each time step of the simulation process.
- (ii) Real and image charges are introduced as point charges, as real 3D or 2D (infinite line) quantities. Hence, it is possible to obtain real 3D boundary conditions at the borders of the integration region. For example, at the plane of symmetry of a streamer channel on a dielectric surface the derivative of the potential along the axis normal to the plane of symmetry is zero. In this case the 3D Poisson equation is reduced to a 2D one, i.e. with precise 3D boundary conditions it is possible to obtain 3D field distributions solving a 2D Poisson equation.

Apart from an exact determination of the field strength, photoionization and photoemission are important for modelling of DBDs. Usually, photoionization is considered as the principal process of pre-ionization, which is necessary for streamer propagation. Photoionization needs, e.g., photons with energies of more than 12.2 eV and 15.6 eV to ionize molecular oxygen and nitrogen, respectively.

As the work function of most materials is in a narrow range between 4 and 6 eV, photons able to release electrons from surfaces must have these energy values, only. Hence, from physical reasons the probability of photoemission and photoionization differs by orders of magnitude; moreover, photons able to cause electron emission are hardly absorbed in the gas volume. However, photoemission is seldom included while modelling DBDs and its role is regarded as negligible (e.g. [36]). This conclusion seems to be valid for the steady state of a discharge, e.g. after the establishment of the cathode layer in VD arrangements. In the cathode-directed streamer

of any configuration of DBDs (at the tip of the channel) ions hardly move and electron emission on surfaces by ion impact does not take place, i.e. photoemission determines the streamer propagation (see e.g. [37, 60] and figure 41). Behind the streamer (in the channel or near the surfaces) all processes occur very slowly and the role of photoemission decreases (compare photo- and ion emission currents in figure 32).

In summary, DBD development along a dielectric surface can be described as the development of channels with finite length, thickness and width (3D objects), which are situated on the dielectric surface (due to the field conditions) and propagate along the surface (due to photoemission processes). These aspects of DBD development near and on surfaces require special attention on the boundary conditions at the dielectric surface. Hence, accurate values of the electric field at the dielectric surface, the consideration of photoemission and photoionization are essential prerequisites for reliable numerical investigations of DBDs.

5.2. General discharge behaviour

The appearance of the DBD in the three basic configurations, i.e. the VD, CD and SD arrangements, looks rather different. However, the analysis of the discharge dynamics leads to the conclusion that there exist a few discharge phenomena, which are common in all arrangements. The importance of the discrete phenomena varies and determines the actual dynamics of the discharge. The sequence of the discharge phases is the same in any configuration, while the structure of the discharge appearance and the quantitative characteristics depend on the specific arrangement.

The common, successive phases of DBDs in all configurations are (i) the Townsend or pre-breakdown phase, (ii) the streamer phase and (iii) the decay phase.

The *first phase* starts when the field strength in the gas approaches the breakdown value. Electron multiplication is

driven by the local field strength. In this phase the overall field strength in the discharge region remains nearly unchanged; the existence of the dielectric barrier does not play any role.

The initial electrons, necessary for the first avalanches, arise from preceding discharge processes or by natural sources. Initial electrons are distributed in the whole gas gap. In some cases the distribution may be nearly homogeneous, in others, not. It depends on the preceding processes, which can leave some irregularities in the discharge region. In this discharge phase the overall field strength distribution is determined by the electrode arrangement, surface charges, and not by discharge processes.

With further electron multiplication the number of electrons reaches the critical value given by the Raether–Meek criterion somewhere in the gas gap, and the transition to a streamer occurs. The discharge dynamics during the *streamer phase* leads to microdischarge channels and cathode layer formation. Depending on the overall discharge dynamics the microdischarge channel can be realized in a constricted form (filamentary) or as a broad discharge structure (homogeneous DBD).

The streamer phase determines the final energy consumption, temperature rise and number of reactive particles generated in the discharge region.

When the electron number locally exceeds the critical number of about 10^8 (Raether–Meek criterion), two types of streamers, the cathode- and anode-directed ones, appear. The cathode-directed streamer propagates towards or along the cathode, while the anode-directed streamer moves towards or along the anode. The anode-directed streamer propagates in the same direction as the electron drift, while the cathode-directed one moves in the opposite direction. This structure, a high-conductive region with two streamers at the opposite ends, is common for DBDs and arises in the streamer phase; it is the microdischarge channel. The discharge channel behaves like a wire in an electric field, with field strength maxima at its tips. The field strength maxima correspond to the streamers. Usually, the cathode-directed streamer is more developed than the anode-directed one.

The third phase, the *decay phase*, comprises the decay of the discharge, which is mainly determined by the movement of ions.

It is necessary to point out that streamers and channels are not compulsorily connected with filamentary DBDs in general. The cross-section of the channel can be much larger than the inter-channel distance, or several channels can develop close to one another and cannot be distinguished experimentally. If not particularly mentioned, the discussion about streamers and channels comprises the filamentary and the homogeneous DBDs.

5.3. Dynamics of the cathode-directed streamer

5.3.1. Mechanism of streamer propagation. The cathode-directed streamer and its propagation are based on electron multiplication. Electrons appear in front of the streamer due to photoionization in the gas space and photoemission on surfaces. Their multiplication in the cathode-directed

streamer is accompanied by the production of photons (e.g. figure 41). These processes, photon production at the centre of the streamer and the appearance of secondary electrons from surfaces, cause a positive feedback resulting in streamer growth and propagation in all basic DBD arrangements (figures 2, 8, 9, 21, 22, 41 and 42, [16, 21–23]).

In order to support the formation and propagation of the cathode-directed streamer two conditions must be fulfilled: a source of electrons in front of the streamer must exist and a specific field configuration, which directs electrons from the source to the streamer (streamer and electrons propagate in reverse directions).

The most important source of electrons in the streamer phase is photoemission from surfaces. Photoionization in the gas region is of less importance (see section 5.1). Other sources, such as the emission of secondary electrons due to the impact of positive ions on the cathode, do not play a comparable role (except in the cathode layer). For example, in SD arrangements (figures 41 and 43(c)), electrons appear in front of the streamer because of photoemission (figures 41 and 43(c)), move to the tip of the channel and multiply their number in the streamer. Their multiplication causes a photon flux to the surfaces. The photons originate from the centre of the streamer (figure 41).

The second requirement is a proper direction of the field strength. In the VD case this is automatically fulfilled, because the streamer in the gas gap and secondary electrons move along the same axis (normal to the surfaces). In SD and CD the directions of streamer propagation and current from electron emission are perpendicular to one another. The cathode-directed streamer moves along the surface while secondary electrons appear on the surface(s). In order to reach the streamer, however, secondary electrons must move along the surface (figures 40, 43 and 46) and, accordingly, a significant field strength component parallel to the cathode surface is required. In the case of the dielectric cathode this field strength component is caused by surface charges (figure 45). Immediately after breakdown the initial field configuration changes due to the collection of surface charges on the dielectric so that secondary electrons reach the streamer. Further streamer development and propagation happen according to the photoemission/electron multiplication mechanism described above.

If the (metallic) surface electrode of an SD arrangement is the cathode, there is no surface charging resulting from the cathode-directed streamer (figure 33). The structures in figures 33 and 43, which move along the surface of the cathode, look rather different; however, both of them are cathode-directed streamers. On conductive surfaces, surface charges cannot exist. Moreover, the field strength component parallel to the conductive surface must be zero just on the surface. In the vicinity of the conductive surface it can be different from zero, only to a limited extent. Hence, the streamer near the conductive cathode is less intensive and its lifetime is short compared with that of those streamers, which propagate along the dielectric cathode. The appearance of the required field configuration (non-zero field component parallel to the surface) is provided by volume charges in the cathode layer and

Table 5. Parameters of a streamer propagating on the dielectric cathode (SD case).

| Time (ns) | 4.9 | 7.2 | 10.5 | 12.1 | 16.3 | 18.6 | 20.4 | 24.7 |
|---|-----|------|------|------|------|------|------|------|
| Field strength maximum (Td) | 150 | 160 | 170 | 180 | 300 | 450 | 500 | 600 |
| Streamer velocity ($\text{cm s}^{-1} \cdot 10^6$) | 0.6 | 0.65 | 1.2 | 1.7 | 1.9 | 5.4 | 7.5 | 12.5 |
| Width of the streamer (μm) | 150 | 122 | 100 | 75 | 75 | 75 | 75 | 75 |

in the conductive channel. But these charges do not support streamer propagation.

5.3.2. Parameters of the cathode-directed streamer.

Although cathode-directed streamers appear in any DBD configuration, they develop differently. In VD and SD arrangements the inter-electrode distance limits their lifetime, e.g. their propagation stops when the surface of the cathode (VD case) and the location of the cathode on the dielectric (CD case) are reached, respectively. In SD arrangements the gap width is not fixed; here the streamer might exist longer (figure 10).

The parameters, which mainly characterize the cathode-directed streamer, are the amplitude of field distortion, streamer size, propagation velocity and the distance, which the streamer bridges. Apart from the distance, which is fixed in VD and CD arrangements, all parameters are not constant during streamer propagation, i.e. only in the SD arrangement the parameters may reach saturation level.

The amplitude of field distortion in the streamer grows continuously starting from the moment of streamer appearance (figures 8, 21, 40 and table 5). The streamer needs about 20 ns to reach saturation conditions in the SD arrangement under the considered boundary conditions (acceleration time). During this acceleration time, the streamer size (width of field distortion) becomes twice as small, the field strength rises fourfold, the streamer velocity increases from $0.6 \times 10^6 \text{ cm s}^{-1}$ to $12.5 \times 10^6 \text{ cm s}^{-1}$ and the streamer moves by about 1 mm (table 5).

During the following 20 ns, up to 45.2 ns in figure 40, the streamer propagates with nearly constant velocity and slowly decreasing field strength maximum. The distributions (charge densities, field strength, etc) in and near the streamer are ‘frozen’; they are shifted from the conductive anode along the dielectric cathode.

At negative polarity of the surface electrode (SD case) the same features are found near the conductive cathode. However, the streamer development stops earlier (no surface charge on the conductive surface). The streamer behaviour is similar at both polarities if either the field strength maxima or the streamer velocity is comparable (the data in table 5 in the time interval from 7 to 12 ns are comparable to those in table 6 between 5 and 8 ns). Unlike the positive polarity of the surface electrode further development of the streamer does not take place; it de-accelerates and disappears within a short time.

In the VD case, as mentioned above, the streamer propagates along the same axis as the electron flux, normal to the surfaces. The streamer leaves a high-conductive region, where the field strength decreases. As the voltage between the electrodes remains practically constant, this decrease in the conductive region causes a rearrangement of the field strength

Table 6. Parameters of a streamer propagating on the conductive cathode (SD case).

| Time (ns) | 5.21 | 6.37 | 8.36 |
|---|------|------|------|
| Field strength maximum (Td) | 128 | 180 | 157 |
| Streamer velocity ($\text{cm s}^{-1} \cdot 10^6$) | | 1.5 | 0.8 |
| Width of the streamer (μm) | 40 | 40 | 40 |

distribution resulting in a certain field strength rise in front of the streamer. This in turn causes continuous streamer acceleration from its appearance (at ~ 10 ns figure 9) up to the time where it reaches the surface of the cathode (~ 12 ns in figure 9).

This acceleration time of 2 ns is not long enough to reach saturation values of the parameters given in table 5. The maximum value of the field strength in the cathode-directed streamer rises continuously and finally reaches the level of the field strength in the cathode layer (figure 10 at 0 ns). In the CD case the short inter-electrode distance leads to an ‘underdeveloped’ cathode-directed streamer as well (figure 21).

The value of the field strength maximum in the streamer is determined by the dynamic equilibrium between the rate of electron generation (multiplication) and the rate of electron loss (by drift) in the streamer on the one hand, and the overall charge and field distribution on the other hand. The equilibrium is associated with the gas properties, while the field distribution depends on the actual discharge condition. For example, near the metallic cathode of an SD arrangement the streamer is less developed and exists for a shorter time while along the dielectric cathode it exists much longer and can bridge a long distance (see data in tables 5 and 6).

5.3.3. Cathode-directed streamer and Lichtenberg figure. In a barrier discharge with a gas gap (VD and CD arrangements) cathode- and anode-directed streamers appear in between the electrodes (figures 6, 9 and 21). After an undisturbed, free movement in the gas gap (figures 2 and 9, 10–13 ns) the cathode-directed streamer reaches the cathode. Further discharge development is connected with cathode layer extension along the cathode surface. The same processes happen in SD arrangements with negative polarity of the dielectric (compare figure 10 with figures 33–35). Finally, the cathode layer radius is about 50–75 μm in VD arrangements at atmospheric pressure (figure 10) and about 60–80 μm in SD arrangements under the same conditions (figures 34 and 35).

In the VD case the microdischarge channel, which is left behind the streamer, is based on the cathode layer. The channel plays the role of a conductive rod, which is pressed to the cathode surface (figure 12). With a dielectric cathode

the microdischarge channel plays the role of a conductive electrode and the situation is similar to SD arrangements with positive polarity of the surface electrode. In SD arrangements a set of microdischarge channels are distributed along the conductive electrode on the dielectric surface (figure 30). In VD arrangements microdischarges diverge radially from the lateral surface of the channel. This set of microdischarge channels around the ‘original’ one is known as the Lichtenberg figure (e.g. figure 3(b)). With conductive cathode the streamer does not split into distinct channels and no Lichtenberg figure appears (compare figure 3(a) with 3(b)), while the cathode layer exists in any case.

The development and propagation of each microdischarge channel belonging to the Lichtenberg figure happen in accordance with the presented mechanism of development and propagation of the cathode-directed streamers in SD arrangements with positive polarity of the surface electrode (figures 40, 41 and 43). The length of such microdischarge channels on the surface is about several millimetres (table 4). In the VD case the cathode-directed streamer does not disappear after reaching the dielectric cathode. It turns along the dielectric surface, propagates radially and forms a homogeneous cathode layer (e.g. figure 10). At further radial propagation the streamer branches into several channels, which encircle the cathode layer, which are known as the Lichtenberg figure.

5.4. Dynamics of the anode-directed streamer

Together with the cathode-directed streamer an anode-directed one appears in all DBD arrangements (e.g. figures 8, 9, 21, 34, 36 simulation and figure 2 experiment). They appear simultaneously somewhere in the gas gap when the electron number reaches the Raether–Meek criterion and propagate to the cathode and anode, respectively.

The anode-directed streamer moves in the same direction as the electron flux. Photoemission and photoionization, which produce electrons in front of the streamer, do not play an essential role, because secondary electrons are extracted from the area in front of the streamer and return to the anode. Electrons which reach the streamer appear in the conductive channel.

Within the conductive channel electron production depends on field strength. Its value follows from the equilibrium between the rate of the electron multiplication and electron attachment processes (in electronegative gases). If occasionally the electron density rises locally, the conductivity rises there as well and the local field strength decreases. At reduced field strength the rate of attachment processes rises and the electron density drops to the previous level, and vice versa. The field strength value belonging to this equilibrium is about 100 Td in oxygen. Exactly this value has been found by modelling for all basic DBD arrangements (figures 12, 21, 37 and 42(b)) and by experiment [16]. As a result, electrons which enter the channel will not significantly change the electron number density within the channel. Because of this the source of electrons feeding the anode-directed streamer is the cathode-directed streamer or the cathode layer.

The value of 100 Td is slightly lower than the breakdown field strength in air and oxygen. The kinetic equilibrium is near 105 Td. The resulting value of field strength in the channel is determined by the equilibrium as well as the dynamics of the charge transfer through the discharge channel. As shown in section 4 there are two possible states in the channel, at a field strength between 80 and 100 Td and at one close to zero. The first one appears if the charge transfer through the discharge channel happens with an electron density not exceeding a certain level (about 10^{13} cm^{-3}). In this case the kinetic equilibrium prevails, the field strength is between 80 and 100 Td and the channel is connected to a comparably weak source of electrons, the cathode layer (or an underdeveloped cathode-directed streamer). With a well-developed cathode-directed streamer the channel is connected to a strong source of electrons, its field strength drops down to zero, the electron density rises up to at least 10^{14} cm^{-3} and the influence of the kinetic processes on the condition (state) of the channel becomes negligible.

Because of the equilibrium in the channel the electron density remains constant in the channel. The channel connects the anode-directed streamer with either the cathode-directed streamer or the cathode layer on the opposite side of the channel (figures 8, 9, 21, 34 simulation and figure 2, [16, 21–23, 26] experiments). In contrast to the anode-directed streamer the cathode-directed one absorbs electrons from any direction (e.g. figure 42). They pass the streamer, multiply their number and are expelled to the channel. The cathode-directed streamer works like a vacuum cleaner, which collects dust (electrons) from any direction and forces it to go through a tube (the microdischarge channel). The electrons pass through the channel and multiply their number in the anode-directed streamer and by this elongate the channel towards the anode.

In the case of a dielectric anode the streamer reaches the surface and radially expands on the dielectric (figures 2(a), 3(a), 12(b) and 13(a) [26]). This propagation happens homogeneously in the radial direction without division into separate channels as on the surface of dielectric cathodes. The amplitude of field distortion in the anode-directed streamer is about 150 Td (VD case, figure 12(b), arrow), which is close to that in the SD case (figure 37). A charged spot appears on the dielectric surface with a cross-section of several millimetres, several times larger than the diameter of the microdischarge channel (figure 2).

The channel equilibrium mentioned above disappears if a highly effective electron source is available, for example, a well-developed cathode-directed streamer. If the electron source is able to deliver electrons with a density an order higher than that of the equilibrium, the field strength in the channel decreases practically to zero (figure 40). If there are no attachment processes, as in electropositive gases, then also the field strength in the channel is close to zero.

5.5. Filamentary and homogeneous discharge structure

Looking at DBDs, filamentary and more homogeneous discharge structures have been observed. The main question is: does there exist any physical mechanism in the discharge

dynamics, which promotes the formation of filamentary or homogeneous discharge structures? The model used to describe DBDs does not include any special physical mechanism, which is responsible for the development of certain discharge structures. The model comprises a general physical description of the movement and multiplication of charged particles in a continuously changing field configuration. Because of this two more questions arise: what does homogeneity mean with respect to channel development obtained from modelling and why does the model provide filamentary structures only?

The answer to the first question is obvious; the homogeneous discharge most probably consists of a set of discharge channels, which develop close to one another. The appearance of the channel structure (second question) has a principal physical reason: the transition from avalanche to streamer cannot happen homogeneously in the whole discharge region. Even at ideal initial field strength distribution the occurrence and number of seed electrons are a question of probability. As a result the transitions happen somewhere locally leading to the development of distinct channels.

To understand the conditions at which filamentary or homogeneous discharge forms appear, it is necessary to find under which circumstances channels can develop next to one another. In principle, four cases have to be considered, the anode, cathode is a dielectric and the anode, cathode is conductive. (Not all of these cases are realizable in all basic DBD configurations.)

Only one of these cases is strongly forcing a filamentary structure: the dielectric anode. The spreading of the anode-directed streamer over the surface of the dielectric anode (e.g. figure 3(a)) results in charging a comparably large area of the dielectric anode, 14–20 times larger than the channel cross-section (figure 13). This surface charge reduces the field strength around the microdischarge channel (shielding effect [26, 61–64]) and suppresses further discharge activity in the direct surroundings of the channel so that a filamentary structure appears. The inter-channel distance (channel density) results from the interaction of the charged area with neighbouring channels (figure 14).

With conductive anode there is no shielding effect. The anode-directed streamer reaches the anode surface and disappears (figure 2(b)). Without surface charge on the anode, there is no interaction and channels may develop close to one another. In this case broad bright regions of discharge activity are observed (e.g. figure 5).

The cathode has no direct influence on the discharge structure, whether the discharge is filamentary or homogeneous. If the cathode is conductive, there is no shielding effect (due to the absence of surface charges on the cathode) and the processes at the anode determine the discharge structure.

With a dielectric anode, Lichtenberg figures appear. It seems that the Lichtenberg figures do not shield the discharge area around the main discharge channel. Experimentally, the inter-channel distance at the dielectric anode side is comparable to or smaller than the extension of the Lichtenberg figures (e.g. figure 3). This implies that channels can develop between the branches of the Lichtenberg figures. From

modelling it follows that the y -component of the field strength in the gas space above the Lichtenberg channels is nearly zero (figure 43(d)). The reason for this is the fact that the total charge density in the main part of the surface branches (together with the surface charge) is close to zero and differs from zero only around the main channel and the channel tip. Apart from this, the Lichtenberg channels can be additional sources of electrons and by this promote the appearance of numerous parallel discharge channels, which cross the gas gap and fill more or less the discharge region homogeneously (figure 5(a)).

Apart from the shielding effect, homogeneous discharge structures (in VD arrangements) are obtainable if the expansion of surface charges on the dielectric can be avoided. In general, this is possible in two ways: by using a conductive electrode or by stopping (limiting) the charge expansion on the dielectric surface. The charge transfer from the channel to the dielectric surface is prevented if the field strength in the channel is close to zero. In this case, charging of the dielectric surface is not supported by charges from the channel.

In this context, the properties of the working gas are of importance. DBDs in electropositive and electronegative gases differ by the value of the equilibrium field strength in the microdischarge channels. In electropositive gases such as noble gases or nitrogen there are no attachment processes and the equilibrium value of the field strength in the channel is nearly zero. The accumulation of surface charges on the dielectric decreases the field strength in the channel. With low field strengths in the channel, already first traces of surface charges on the anode decrease the field strength in the channel to zero and by this stop further charge transport. As a result, a wide surface charge zone around the channel does not appear, i.e. no shielding effect exists and the DBD may develop in a homogeneous mode even with dielectric anodes (figure 7 [25]).

In electronegative gases, however, the existence of the equilibrium between attachment and ionization processes leads to high field strength in the discharge channel (see the previous section), and the shielding effect is necessary to get homogeneous discharge structures.

Up to now, isotropic initial conditions have been considered. In reality, however, imperfections of surfaces, residual charges and excited particles in the gas space from preceding discharge activities especially at ac operation exist and may influence the overall discharge behaviour. This influence is known as the memory effect on surfaces and in the gas space (e.g. [61–65]). In general this effect leads to the appearance of inhomogeneity in the discharge region and a constriction of discharge areas (filamentary structure). A rise in frequency has a similar effect. If the period of the applied voltage becomes comparable to the relaxation time of the excited particles or lifetime of charge carriers, the discharge can be fixed at certain locations.

There exist another view on the mechanism of controlling the homogeneity during breakdown and discharge development [66]. In [66] the authors analyse several works and believe that certain conditions (Townsend breakdown, no avalanche development, a high ratio of the secondary emission to the ionization coefficient and so on) stimulate homogeneous discharge patterns. They state that during

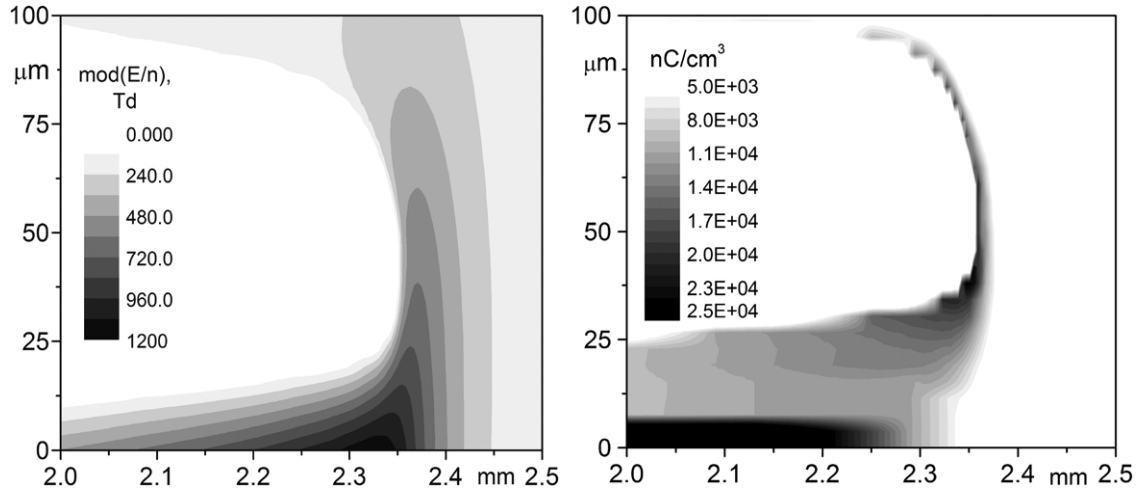


Figure 49. Field strength (*a*) and charge density (*b*) distribution in the vicinity of the cathode-directed streamer (SD arrangement, positive polarity of the surface electrode, $t = 38.8$ ns).

discharge development the homogeneity is controlled mainly by the electrical circuit, the electrode configuration and by the ability of the gas to be slowly ionized (e.g. by Penning ionization).

5.6. Cathode layer

The existence of the cathode layer in a VD arrangement has been proved experimentally [16]. The cathode layer development begins when the cathode-directed streamer reaches the surface of the cathode in the VD case (figures 9 and 10) or starts its propagation along the cathode surface in the CD (figure 22) and SD cases (figures 33, 35 and 41), respectively. The parameters of the cathode layer in all arrangements are close to that of normal glow discharges in oxygen of atmospheric pressure (current density about 250 A cm^{-2} , maximum value of the field strength 1300 Td, layer thickness about $20 \mu\text{m}$ and voltage drop 450 V).

The cathode layer is a source of electrons, which feeds the microdischarge channel and consequently supports the continuity of the current flow. A cathode layer expansion along the cathode surface is observed in all basic DBD arrangements. The amplitude of the discharge current determines the size of the cathode layer and vice versa (constant current density). Moreover, the rate of increase in the cathode layer area defines the rate of rise in the discharge current. With charge accumulation in the gas gap and on the dielectric surface(s) the cathode layer stops its expansion. During further discharge development the size of the layer remains constant, while the maximum field strength and the current density in the layer continuously decrease.

In SD arrangements a movable cathode layer is linked with the channel development along the surface of the dielectric cathode. The layer develops below the cathode-directed streamer (figure 49). The maximum field strength is close to 1300 Td at 2.30–2.35 mm in figure 49(*a*). Its length on the x -axis is less than 0.3 mm; at this length the field strength decreases from 1300 to about 100 Td (figure 49(*a*)) because of charge accumulation (figure 49(*b*)). This cathode layer moves

together with the streamer. This means that the lifetime of the movable cathode layer at a certain place below the streamer is about 3 ns (with the value of the streamer velocity given in table 5).

5.7. Microdischarge channel

The development of the anode- and cathode-directed streamers results in the appearance of a microdischarge channel with comparatively high conductivity in between the streamers (e.g. figures 12, 21 and 23 VD case; figures 36 and 46 SD case). The channel is practically neutral and its conductivity depends on the charge carrier density and their mobility. The charge carrier density in the channel is determined by the productivity of the electron source, which feeds the channel. Initially, the only electron source is the cathode-directed streamer. The anode-directed streamer is a consumer of electrons from the channel. The cathode layer can substitute the cathode-directed streamer during further discharge development.

The cathode layer and underdeveloped cathode-directed streamers are no powerful electron sources. The charge carrier density in the channel is determined by the already mentioned equilibrium between the rate of electron multiplication and attachment processes. The resulting parameters of the equilibrium in the channel are the following (for oxygen and air): field strength about 100 Td and electron and positive ion density about 10^{13} cm^{-3} (figure 23 or 42(*c*) and (*d*)). If the cathode-directed streamer becomes more developed, the electron density in the channel rises to 10^{16} cm^{-3} (figures 43(*c*) and (*d*)) and the equilibrium in the channel disappears. Correspondingly, the high electron density reduces the field strength in the channel to practically zero (figure 40). A certain time duration is necessary for this development or, in other words, a certain channel length. The length of the channels, for example, along the dielectric surface, depends on the internal channel parameters. If the mean field strength in the channel is about 100 Td, its length cannot exceed a level of 1 mm, because the potential of the streamer (or the channel tip) decreases by 3 kV per mm channel length according to Paschen's law under

normal conditions. Additionally, there is a 0.5 kV drop in the cathode layer. These values in total are comparable to the breakdown voltage, which is about 3.3 kV (at normal pressure) for SDs (table 4) and for VDs with a 1 mm gas gap (figure 13).

With a well-developed cathode-directed streamer, the field strength in the main part of the discharge channel is close to zero (figure 40) with a certain increase in the field strength near the conductive anode. With near-zero field strength in the channel the potential in the streamer remains close to that of the conductive anode. It decreases from 3.3 to 1.5 kV within the channel length of about 3.5 mm (figure 40). And this is the reason for the appearance of long channels in the Lichtenberg figures.

6. Conclusions

DBDs in any arrangement consist of cathode- and anode-directed streamers, discharge channels, cathode layers and charged surfaces. The development and interaction of these items together with the actual boundary conditions determine the parameters of gas breakdown, which are essential for the effectiveness of specific DBD applications.

Energetic processes in DBDs (of any arrangement) start with the appearance of the cathode-directed streamer. The cathode-directed streamer is a self-sustaining phenomenon, which moves in the gas gap or along electrodes. The mechanism of the movement and development of the cathode-directed streamer is a positive feedback between photoemission electrons (from surfaces) and their further multiplication in the streamer with simultaneous photon production.

The cathode-directed streamer develops in time and may reach saturation conditions. For example, in oxygen under normal conditions, maximum values of the field strength, charged particle density, streamer velocity and so on are reached within 10–15 ns.

The cathode-directed streamer is connected with the anode-directed one by a highly conductive discharge channel. The anode-directed streamer plays a subsidiary role; it cannot support its own development.

The parameters of the conductive channel depend on the productivity of the electron source, which feeds the channel. With ‘moderate’ electron sources (cathode layer or not fully developed cathode-directed streamer) the electron density in the channel is determined by the equilibrium between the rates of electron attachment and ionization processes. The field strength belonging to this equilibrium in oxygen and air under normal conditions is close to 100 Td. With a continuously developing cathode-directed streamer, the equilibrium disappears and the field strength becomes close to zero. In electropositive gases, such as nitrogen and noble gases, attachment processes do not exist and the related equilibrium field strength is close to zero.

A cathode layer appears when the cathode-directed streamer touches the surface of the electrode. The parameters of this layer are close to those of normal glow discharges. In the case of a conductive cathode, the cathode layer is stationary while with a dielectric cathode it moves together with the

streamer and disappears due to charge accumulation on the surface. In VD arrangements the streamer propagation along the dielectric surface results in the appearance of Lichtenberg figures.

In VD arrangements (with dielectric anode) a filamentary discharge structure appears in electronegative gases due to a shielding effect. Charge carriers approaching the anode spread on the dielectric anode and the field strength in the vicinity of the channel in the gas gap decreases. Because of this, further discharge processes are suppressed in this area (no field—no discharge) and the discharge on the dielectric surface exhibits a filamentary structure. Without the shielding effect (e.g. with a conductive anode or in electropositive gases) discharge processes can take place close to one another so that homogeneous discharge structures may appear.

References

- [1] Massines F *et al* 1998 Experimental and theoretical study of a glow discharge at atmospheric pressure controlled by dielectric barrier *J. Appl. Phys.* **83** 62950–7
- [2] Massines F and Gouda G 1998 A comparison of polypropylene-surface treatment by filamentary, homogeneous and glow discharges in helium at atmospheric pressure *J. Phys. D: Appl. Phys.* **31** 3411–20
- [3] Massines F *et al* 2003 Physics and chemistry in a glow dielectric barrier discharge at atmospheric pressure: diagnostics and modeling *Surf. Coat. Technol.* **174** 8–14
- [4] Celestin S *et al* 2008 Influence of the charges deposition on the spatio-temporal self-organization of streamers in a DBD *J. Phys. D: Appl. Phys.* **41** 205214
- [5] Celestin S *et al* 2009 Influence of surface charges on the structure of a dielectric barrier discharge in air at atmospheric pressure: experiment and modelling *Eur. Phys. J. Appl. Phys.* **47** 22810
- [6] Papageorgiou L *et al* 2009 Two-dimensional modeling of a nitrogen dielectric barrier discharge (DBD) at atmospheric pressure: filament dynamics with the dielectric barrier on the cathode *J. Phys. D: Appl. Phys.* **42** 105201
- [7] Merbah N, Sewraj N, Marchal F, Salamero Y and Millet P 2004 Luminescence of argon in a spatially stabilized mono-filamentary dielectric barrier micro-discharge: spectroscopic and kinetic analysis *J. Phys. D: Appl. Phys.* **37** 1664–78
- [8] Nishida H and Abe T 2011 Numerical analysis of plasma evolution on dielectric barrier discharge plasma actuator *J. Appl. Phys.* **110** 013302
- [9] Sewraj N, Merbah N, Gardou J P, Rodriguez Akerreta P and Marchal F 2011 Electric and spectroscopic analysis of a pure nitrogen mono-filamentary dielectric barrier discharge *J. Phys. D: Appl. Phys.* **44** 145201
- [10] Xu X P and Kushner M J 1998 Multiple microdischarge dynamics in dielectric barrier discharges *J. Appl. Phys.* **84** 4153–60
- [11] Xu X P and Kushner M J 1998 Ion composition of expanding microdischarges in dielectric barrier discharges *J. Appl. Phys.* **83** 7522–32
- [12] Lee D, Park J M, Hong S H and Kim Y 2005 Numerical simulation on mode transition of atmospheric dielectric barrier discharge in helium–oxygen mixture *IEEE Trans. Plasma Sci.* **33** 949–57
- [13] Wagner H-E, Brandenburg R, Rozlov KV, Sonnenfeld A, Michel P and Behnke J F 2003 The barrier discharge: basic properties and applications to surface treatment *Vacuum* **71** 417–36

- [14] Kozlov K V, Brandenburg R, Wagner H-E, Morozov A M and Michel P 2005 Investigation of the filamentary and diffuse mode of barrier discharges in N₂/O₂ mixtures at atmospheric pressure by cross-correlation spectroscopy *J. Phys. D: Appl. Phys.* **38** 518–29
- [15] Kozlov K V and Wagner H-E 2007 Progress in spectroscopic diagnostic of barrier discharges *Contrib. Plasma Phys.* **47** 26–33
- [16] Hoder T, Brandenburg R, Basner R, Weltmann K-D, Kozlov K V and Wagner H-E 2010 A comparable study of three different types of barrier discharge in air at atmospheric pressure by cross-correlation spectroscopy *J. Phys. D: Appl. Phys.* **43** 124009
- [17] Brandenburg R, Wagner H-E, Morozov A M and Kozlov K V 2005 Axial and radial development of microdischarges of barrier discharge in N₂/O₂ mixtures at atmospheric pressure *J. Phys. D: Appl. Phys.* **38** 1649–57
- [18] Boeuf J P, Punset C, Hirech A and Doyeux H 1997 Physics and modeling of plasma display panels *J. Phys. IV C* **4** 3–14
- [19] Fiala A, Pitchford L C and Boeuf J P 1994 Two-dimensional hybrid model of low-pressure glow discharge *Phys. Rev. E* **49** 5607–22
- [20] Punset C, Boeuf J P and Pitchford L C 1998 Two-dimensional simulation of an alternating current matrix plasma display cell: cross-talk and other geometric effects *J. Appl. Phys.* **83** 1884–97
- [21] Heuser C and Pietsch G 1981 Comparison of gas discharge forms producing ozone *Proc. 5th Int. Symp. on Plasma Chemistry (Edinburgh, UK)* pp 433–8
- [22] Heuser C and Pietsch G 1980 Prebreakdown phenomena between glass–glass and glass–metal electrodes *6th Int. Conf. on Gas Discharges and their Applications (Edinburgh, UK) IEE Conf. Publ.* **189** 98–101
- [23] Heuser C and Pietsch G 1983 Temporal and spatial resolved photometrical measurements of the ozone concentration in a model ozonizer *Proc. 6th Int. Symp. on Plasma Chemistry (Montreal, Canada)* pp 675–80
- [24] Drimal J, Gibalov V I and Samoilovich V G 1987 The magnitude of the transferred charge value in the silent discharge in oxygen *Czech. J. Phys. B* **37** 1248–55
- [25] Drimal J, Gibalov V I and Samoilovich V G 1987 Silent discharge in air, nitrogen and argon *Czech. J. Phys. B* **37** 641–4
- [26] Braun D, Gibalov V and Pietsch G 1992 Two-dimensional modelling of the dielectric barrier discharge in air *Plasma Sources Sci. Technol.* **1** 166–74
- [27] Rauf S and Kushner M 1999 Dynamics of coplanar-electrode plasma display panel cell: I. Basic operation *J. Appl. Phys.* **85** 3460–9
- [28] Rauf S and Kushner M 1999 Dynamics of coplanar-electrode plasma display panel cell: II. Cell optimization *J. Appl. Phys.* **85** 3470–6
- [29] Rauf S and Kushner M J 1999 Operation of a coplanar-electrode plasma discharge panel cell *IEEE Trans. Plasma Sci.* **27** 10–11
- [30] Boeuf J P, Punset C, Hirech A and Doyeux H 1997 Physics and modelling of plasma display panels *J. Phys. IV C* **4** 3–14
- [31] Guo J-M 1993 Two-dimensional nonequilibrium fluid model for streamers *IEEE Trans. Plasma Sci.* **21** 684–95
- [32] Ventzek P L G, Sommerer T J, Hoekstra R J and Kushner M J 1993 Two-dimensional hybrid model of inductively coupled plasma sources for etching *Appl. Phys. Lett.* **63** 605–7
- [33] Punset C, Cany S and Boeuf J P 1999 Addressing and sustaining in alternating current coplanar plasma display panels *J. Appl. Phys.* **86** 124–33
- [34] Cho T-S, Ko J-J, Kim Dae-II, Lee C-W, Cho G and Choi E-H 2000 Influence of sustaining pulse-width on electro-luminous efficiency in ac plasma display panels *Japan. J. Appl. Phys.* **39** 4176–80
- [35] Braun D, Küchler U and Pietsch G J 1991 Microdischarges in air-fed ozonizer *J. Phys. D: Appl. Phys.* **24** 564–72
- [36] Kushner M J 2005 Modelling of microdischarge devices: plasma and gas dynamics *J. Phys. D: Appl. Phys.* **38** 1633–43
- [37] Bhoj A N and Kushner M J 2004 Avalanche process in an idealized lamp: II. Modelling of breakdown in Ar/Xe electric discharges *J. Phys. D: Appl. Phys.* **37** 2510–26
- [38] Eliasson B and Kogelschatz U 1986 Basic data for modelling of electric discharges in gases: oxygen *Brown Boveri Research Report KLR 86-11 C*
- [39] Book D L, Boris J P and Hain K 1975 Flux-corrected transport: II. Generalizations of the method *J. Comput. Phys.* **20** 248–83
- [40] Georghiou G E, Morrow R and Metaxas A C 1999 An improved finite element flux-corrected transport algorithm *J. Comput. Phys.* **148** 605–20
- [41] Georghiou G E, Morrow R and Metaxas A C 2000 A two-dimensional, finite element, flux-corrected transport algorithm for solution of gas discharge problems *J. Phys. D: Appl. Phys.* **33** 2453–66
- [42] Sweet R 1977 A cyclic reduction algorithm for solving block tridiagonal systems of arbitrary dimensions *SIAM J. Numer. Anal.* **14** 706–20
- [43] Hoder T *et al* 2009 3D imaging of the single microdischarge development in coplanar barrier discharges in synthetic air at atmospheric pressure *Contrib. Plasma Phys.* **49** 6381–7
- [44] Hoder T *et al* 2008 Investigation of the coplanar barrier discharge in synthetic air at atmospheric pressure by cross-correlation spectroscopy *J. Phys. D: Appl. Phys.* **41** 035212
- [45] Gibalov V I and Pietsch G J 2004 Dynamics of dielectric barrier discharges in coplanar arrangements *J. Phys. D: Appl. Phys.* **37** 2082–92
- [46] Simek M, Prukner V and Schmidt J 2011 Optical and electrical characteristics of a single surface DBD micro-discharge produced in atmospheric-pressure nitrogen and synthetic air *Plasma Sources Sci. Technol.* **20** 025009
- [47] Hulkula L and Pietsch G J 2002 On the ignition voltage and structure of coplanar barrier discharges *Contributed Papers of Int. Symp. on High Pressure, Low Temperature Plasma Chemistry (HAKONE VIII) (Pühajärve, Estonia)* vol II, pp 259–63
- [48] Murata T, Okita Y and Terai K 1997 Distribution of surface discharge for ozone generation *Proc. 23rd Int. Conf. on Phenomena in Ionized Gases (Toulouse, France)* vol III, pp 82–3
- [49] Gibalov V I and Pietsch G J 2004 Properties of dielectric barrier discharges in extended coplanar electrode systems *J. Phys. D: Appl. Phys.* **37** 2093–100
- [50] Gibalov V I, Murata T and Pietsch G J 2000 Modelling of the discharge development in coplanar arrangements *Proc. 13th Int. Conf. on Gas Discharges and their Applications (Glasgow, UK)* vol I, pp 275–8
- [51] Gibalov V I, Murata T and Pietsch G J 2002 Some characteristic parameters of coplanar discharge arrangements *Proc. 14th Int. Conf. on Gas Discharges and their Applications (Liverpool, UK)* vol I, pp 183–6
- [52] Takeshi T and Ryozo Is 1978 Electric fields in dielectric multi-layers calculated by digital computer *IEEE Trans. Electr. Insul.* **EI-13** 37–44
- [53] Likhanskii A V, Semak V V, Shneider M N, Opaits D F, Miles R B and Macheret S O 2009 The role of the photoionization in the numerical modeling of the DBD plasma actuator *47th AIAA Aerospace Sciences Meeting*

- Including The New Horizons Forum and Aerospace Exposition (Orlando, FL, 5–8 January 2009)* AIAA 2009-841
- [54] Unfer T and Boeuf J P 2009 Modelling of a nanosecond surface discharge actuator *J. Phys. D: Appl. Phys.* **42** 194017
- [55] Takashima K (Udagawa), Zuzeek Yv, Lempert R W and Adamovich Ig V 2011 Characterization of a surface dielectric barrier discharge plasma sustained by repetitive nanosecond pulses *Plasma Sources Sci. Technol.* **20** 055009
- [56] Gibalov V I and Pietsch G J 2000 The development of the dielectric barrier discharges in gas gap and on the surfaces *J. Phys. D: Appl. Phys.* **33** 2618–36
- [57] Pietsch G J and Saveliev A 2002 Some properties of the barrier discharges on the dielectric surfaces *Proc. 14th Int. Conf. on Gas Discharges and their Applications (Liverpool, UK)* vol 1, pp 183–6
- [58] Chao Li, Ebert U and Husdorfer W 2010 Spatially hybrid computations for streamer discharges with genetic features of pulled fronts: I. Planar fronts *J. Comput. Phys.* **229** 200–20
- [59] Lay B, Moss R S, Rauf S and Kushner M J 2003 Breakdown processes in metal halide lamps *Plasma Sources Sci. Technol.* **12** 8–21
- [60] Kushner M J 2004 Modeling of microdischarge devices: pyramidal structures *J. Appl. Phys.* **95** 846–59
- [61] Brauer I, Punset C, Purwans H-G and Boeuf J P 1999 Simulations of self-organized filaments in a dielectric barrier glow discharge plasma *J. Appl. Phys.* **85** 7569–72
- [62] Muller L, Punset C, Ammelt E, Purwans H-G and Boeuf J P 1999 Self-organized filaments in dielectric barrier glow discharges *IEEE Trans. Plasma Sci.* **27** 20–1
- [63] Kogelschatz U 2002 Filamentary, patterned, and diffuse barrier discharges *IEEE Trans. Plasma Sci.* **30** 1400–8
- [64] Radu I, Bartnikas R, Czeremuszkin Gr and Wertheimer M R 2003 Diagnostics of dielectric barrier discharges in noble gases: atmospheric pressure glow and pseudoglow discharges and spatio-temporal patterns *IEEE Trans. Plasma Sci.* **1** 411–21
- [65] Akishev Y, Aponin Gr, Balakirev A, Grushin M, Karalnik V, Petryakov A and Trushkin N 2011 ‘Memory’ and sustention of microdischarges in a steady-state DBD: volume plasma or surface charge *Plasma Sources Sci. Technol.* **20** 024005
- [66] Massines F, Gherardi N, Naudé N and Ségré P 2009 Recent advances in the understanding of homogeneous dielectric barrier discharges *Eur. Phys. J. Appl. Phys.* **47** 22805